Research Article

Evaluation of an *In Vitro* Three-Dimensional HepaRG Spheroid Model for Genotoxicity Testing Using the High-Throughput CometChip Platform

Ji-Eun Seo[1], Xiaobo He[2], Levan Muskhelishvili[3], Pritpal Malhi[3], Nan Mei[1], Mugimane Manjanatha[1], Matthew Bryant[2], Tong Zhou[4], Timothy Robison[5] and Xiaoqing Guo[1]

[1]Division of Genetic and Molecular Toxicology, National Center for Toxicological Research, U.S. Food and Drug Administration, Jefferson, AR, USA; [2]Office of Scientific Coordination, National Center for Toxicological Research, U.S. Food and Drug Administration, Jefferson, AR, USA; [3]Toxicologic Pathology Associates, Jefferson, AR, USA; [4]Center for Veterinary Medicine, U.S. Food and Drug Administration, Rockville, MD, USA; [5]Center for Drug Evaluation and Research, U.S. Food and Drug Administration, Silver Spring, MD, USA

Abstract

Three-dimensional (3D) culture systems are increasingly being used for genotoxicity studies due to improved cell-to-cell interactions and tissue-like structures that are limited or lacking in 2D cultures. The present study optimized a 3D culture system using metabolically competent HepaRG cells for *in vitro* genotoxicity testing. 3D HepaRG spheroids, formed in 96- or 384-well ultra-low attachment plates, were exposed to various concentrations of 34 test articles, including 8 direct-acting and 11 indirect-acting genotoxicants/carcinogens as well as 15 compounds that show different genotoxic responses *in vitro* and *in vivo*. DNA damage was evaluated using the high-throughput CometChip assay with concurrent cytotoxicity assessment by the ATP assay in both 2D and 3D cultures. 3D HepaRG spheroids maintained a stable phenotype for up to 30 days with higher levels of albumin secretion, cytochrome P450 gene expression, and enzyme activities compared to 2D cultures. 3D spheroids also demonstrated a higher sensitivity than 2D cultures for detecting both direct- and indirect-acting genotoxicants/carcinogens, indicating a better prediction of *in vivo* genotoxicity responses. When DNA damage dose-response data were quantified using PROAST software, 3D spheroids generally had lower or similar benchmark dose values compared to 2D HepaRG cells and were more comparable with primary human hepatocytes. These results demonstrate that 3D models can be adapted to the CometChip technology for high-throughput genotoxicity testing and that 3D HepaRG spheroids may be used as a reliable and pragmatic *in vitro* approach to better support the hazard identification and risk assessment of potential human genotoxic carcinogens.

1 Introduction

Improving current *in vitro* genotoxicity tests to closely mimic human responses is an ongoing task to improve hazard identification and risk assessment (Pfuhler et al., 2011). To increase the ability of *in vitro* mammalian cell genotoxicity tests to reliably predict genotoxicity in humans, recommendations have been made to use human-derived, tumor protein p53-proficient, and metabolically competent cells within the context of appropriately set limits of concentration and cytotoxicity (Kirkland, 2011; Kirkland et al., 2007).

Recently, the human hepatoma-derived HepaRG cell line, which expresses various levels of phase I and phase II enzymes, transporters, and nuclear receptors, has been cited as a promising cell model to be used as a surrogate for primary human hepatocytes (PHHs) for *in vitro* genotoxicity assessments (Guillouzo et al., 2007; Pfuhler et al., 2011). Our previous studies demonstrated that when cultured in 2D format, metabolically competent HepaRG cells expressed significantly higher levels of cytochrome P450 (CYP450) enzyme activities and showed higher sensitivity in detecting DNA damage and the micronuclei (MN) formation induced by a number of genotoxicants or carcinogens

Disclaimer: This manuscript reflects the views of the authors and does not necessarily reflect those of the U.S. Food and Drug Administration.

Received January 12, 2022; Accepted March 16, 2022;
Epub March 18, 2022; © The Authors, 2022.

ALTEX 39(4), 583-604. doi:10.14573/altex.2201121

Correspondence: Xiaoqing Guo; PhD
Division of Genetic and Molecular Toxicology
National Center for Toxicological Research, U.S. Food and Drug Administration
14-1081, 3900 NCTR Road
Jefferson, AR 72079, USA
(Xiaoqing.Guo@fda.hhs.gov)

when compared to HepG2 cells despite both cell lines being derived from human hepatoma (Guo et al., 2020; Seo et al., 2019). 2D HepaRG cells, however, were not as sensitive as PHHs in detecting DNA damage responses induced by 10 genotoxicants or carcinogens (Seo et al., 2020).

Three-dimensional (3D) cell culture systems have been increasingly recognized as better than traditional 2D monolayer culture systems for mimicking human *in vivo* exposures due to their improved cell-to-cell interactions and tissue-like structures (Edmondson et al., 2014; Lauschke et al., 2016). It has been demonstrated that the environment of 3D culture is morphologically, physiologically, and functionally distinct from 2D culture (Baharvand et al., 2006). The International Workshop on Genotoxicity Testing (IWGT) agreed that 3D tissue-based models provide more *in vivo*-like responses in terms of cell viability, proliferation, differentiation, morphology, gene and protein expression, and function compared to standard 2D static cell culture systems (Pfuhler et al., 2020). Once validated, 3D models could be used as 2nd tier assays to follow-up endpoint-specific positives from a standard *in vitro* genotoxicity testing battery. The workshop also suggested that 3D liver model-based genotoxicity assays are promising but only at an early stage of development.

3D spheroids derived from human hepatic cells have gained increasing interest for genotoxicity screening due to their improved metabolic activity and hepatic function compared to 2D monolayer cultures. HepG2 spheroids have been the most reported 3D hepatic model for genotoxicity assessment. Following 24-h treatment, HepG2 spheroids showed higher sensitivity than HepG2 in 2D format in MN induction by benzo[*a*]pyrene (B[*a*]P), 2-amino-1-methyl-6-phenylimidazo(4,5-b) pyridine (PhIP), aflatoxin B1 (AFB1), and methyl methanesulfonate (MMS) using the cytokinesis-block MN assay (Conway et al., 2020; Shah et al., 2018). In addition, 3D HepG2 spheroids were shown to be more sensitive than 2D HepG2 cells to detect DNA damage induced by MMS, B[*a*]P, and two heterocyclic aromatic amines (HAAs) (PhIP and 2-amino-3-methyl-3H-imidazo[4,5-f]quinoline (IQ)) in the comet assay (Elje et al., 2019; Stampar et al., 2019).

A recent study successfully adapted the standard comet assay for use with 3D HepaRG spheroids developed in ultra-low attachment (ULA) plates (Mandon et al., 2019). By evaluating 11 compounds, the authors concluded that 3D HepaRG spheroids were more suitable than 2D differentiated HepaRG cells to detect DNA damage induced by human indirect-acting carcinogens (requiring metabolic activation), especially for compounds metabolized by CYP2E1 and 1A2.

Although 3D cell cultures are being successfully used for genotoxicity studies, applying 3D culture models in high-throughput genotoxicity assays is still challenging. Generally, 3D culture-based assays are considered more difficult to perform, more expensive, and their throughput is lower than that of assays performed in 2D cultures (Pfuhler et al., 2020). Several methods have been established for developing 3D culture models, such as forced-floating, hanging drop, ULA plates, agitation-based approaches, matrices, scaffolds, and microfluidic systems (Breslin and O'Driscoll, 2013; Ivanov et al., 2014). The present study used 96- or 384-well ULA plates to develop 3D spheroids since it is relatively easy to culture highly uniform spheroids in a high-throughput manner versus other methods (Ivanov et al., 2014). In addition, the 96-well CometChip platform, a recently developed high-throughput version of the comet assay, provides a rapid and sensitive method of measuring DNA damage with better reproducibility (Chao and Engelward, 2020). We envisioned that integration of the two technologies may improve the throughput of 3D assays significantly.

In the present study, HepaRG cells were used for developing 3D spheroids with the assumption that this model may generate data that is relevant to the human physiological condition. We optimized and evaluated the 3D HepaRG spheroids for genotoxicity testing by detecting DNA damage responses induced by 34 test articles: 8 direct-acting and 11 indirect-acting genotoxicants or carcinogens as well as 15 compounds that show different genotoxic responses *in vitro* and *in vivo* (Tab. 1). A wide range of concentrations was used to generate a large number of data points indicative of chemical-induced DNA damage, facilitating quantitative benchmark dose (BMD) analysis (Seo et al., 2019; Wills et al., 2016). The resulting BMDs and their upper and lower 90% confidence intervals (BMDU and BMDL) were compared with those calculated using the CometChip data generated from 2D HepaRG cells and PHHs from our previous studies (Seo et al., 2019, 2020).

2 Materials and methods

2.1 Chemicals

Eight direct-acting and 11 indirect-acting genotoxicants/carcinogens as well as 15 compounds that show different genotoxic responses *in vitro* and *in vivo* (Tab. 1) were selected for the *in vitro* genotoxicity test. Seven chemicals, including phenacetin, bupropion, diclofenac, omeprazole, dextromethorphan, chlorzoxazone, and midazolam, were used for CYP450 enzyme substrate cocktails. The metabolites (4-acetamidophenol (APAP), hydroxybupropion (Bup-OH), 4-hydroxy diclofenac (Dic-OH), 5-hydroxy omeprazole (OPZ-OH), dextrorphan (Dex), 6-hydroxy chlorzoxazone (Chlorz-OH), and 1-hydroxymidazolam (Mid-OH)) and internal standard (hydroxybupropion-d6 (Bup-OH-D6)) were used for CYP450 activity measurement. All compounds were purchased from Sigma-Aldrich (St. Louis, MO, USA), except for IQ and PhIP, which were obtained from Toronto Chemical Research (Toronto, ON, Canada).

2.2 Cell culture

The basic medium consisted of William's E medium (Thermo Fisher, Waltham, MA, USA) supplemented with 2 mM GlutaMax™ (Thermo Fisher) and 100 µg/mL primocin (InvivoGen, San Diego, CA, USA). The growth and differentiation media were prepared by adding Growth Medium Supplement (Cat# ADD711C) and Differentiation Medium Supplement (Cat# ADD721C) (Lonza, Walkersville, MD, USA), respectively, to the basic medium. Undifferentiated HepaRG human hepatoma cell line (HPR101) was obtained from Biopredic International (Saint Grégoire, France). Cells were cultured and differentiated at 37°C in a humidified atmosphere with 5% CO_2 according to the supplier's protocol with minor modifications.

Tab. 1: Reported genotoxicity and carcinogenicity of test chemicals

Group	Chemical	CAS#	Ames	Genotoxicity assay findings		Carcinogenicity[a]	References
				In vitro	*In vivo*		
Direct-acting genotoxicants/ carcinogens	4-NQO	56-57-5	(+)	(+) for CA, MLA, pig-a, comet	(+) for MN, pig-a, TG	(+) for oral tumor	Le Hegarat et al., 2014; Dertinger et al., 2012; David et al., 2018; Kanojia and Vaidya, 2006
	$CdCl_2$	10108-64-2	(+/–)	(+) for MN, CA, MLA, HPRT, comet	(+) for CA and MN, comet in liver	(+) for lung, prostate, etc.; Group 1	Kirkland et al., 2016; Guo et al., 2016; Seo et al., 2019
	Cisplatin	15663-27-1	(+)	(+) for MN, pig-a, comet	(+) for MN, pig-a, TG	(+) for lung tumor, leukemia; Group 2A	Bhalli et al., 2013; Dertinger et al., 2019; Bemis et al., 2018
	Colchicine	64-86-8	(–)	(+) for MN, CA, MLA, (–) for comet	(+) for MN in BM and liver	No adequate studies	Kirkland et al., 2016; FDA/CDER, 2013; Seo et al., 2020
	ENU	759-73-9	(+)	(+) for MLA, CA, MN, pig-a, HPRT, comet, UDS	(+) for CA, MN, pig-a, TG, comet	(+) for kidney, mammary tumor, etc.; Group 2A	David et al., 2018; Dertinger et al., 2012; Habas et al., 2017; Kirkland et al., 2016; Le Hegarat et al., 2014; Seo et al., 2019, 2020; Bemis et al., 2018
	Etoposide	33419-42-0	(+)	(+) for MLA, CA, MN, SCE, HPRT, comet; (–) for pig-a	(+) for MN and CA; (–) for TG and pig-a	Increased risk for acute myeloid leukemia in human; Group 2A	Kirkland et al., 2016; David et al., 2018; Yamamoto and Wakata, 2016; IARC, 2000
	HQ	123-31-9	(–)	(+) for MLA, MN, CA, comet	(+) for CA, MN, (–) for comet and TG in liver and stomach	(+) for liver and kidney adenoma; Group 3	IARC, 1999; Kirkland et al., 2016; Peng et al., 2013
	MMS	66-27-3	(+)	(+) for MLA, CA, MN, pig-a, HPRT, comet, UDS	(+) for CA, MN, UDS, pig-a, TG, comet	(+) for nasal, nervous system tumor, etc.; Group 2A	Habas et al., 2017; Liu et al., 2019; Kirkland et al., 2016; Seo et al., 2019, 2020; Dertinger et al., 2012; Bemis et al., 2018
Indirect-acting genotoxicants/ carcinogens	2,4-DAT	95-80-7	(+)	(+) for MLA, CA, MN, comet, UDS, but (-) for comet in HepaRG and HPRT	(+) for UDS and comets, but (+/–) for MN in BM	(+) for liver tumor; Group 2B	Le Hegarat et al., 2014; Severin et al., 2005; Seo et al., 2019, 2020; Kirkland et al., 2016; Guo et al., 2020
	2-AAF	53-96-3	(+)	(+) for MLA and UDS, but (-) for comet in HepaRG	(+) for MN, CA, UDS, γ-H_2AX, TG; (+/–) for comet;	(+) for liver, bladder, mammary gland, and skin tumors	Kirkland et al., 2016; Shigano et al., 2016; OECD, 2020

Group	Chemical	CAS#	Ames	Genotoxicity assay findings		Carcinogenicity[a]	References
				In vitro	*In vivo*		
				and HPRT	(–) for pig-a after single dose, but (+) after 28-day exposure		
	Acrylamide	79-06-1	(–)	(+) for MLA, SCE, CA, but (–) for UDS	(+) for UDS, comet, TG, SCE, MN, CA	(+) for thyroid, mammary, uterine, lung, and glial tumor; Group 2A	IARC, 1994
	AFB1	1162-65-8	(+)	(+) for CA, MN, UDS, HPRT mutations	(+) for MN, CA, UDS, TG in liver, pig-a after 28-day exposure; (–) for comet	(+) for liver, large intestine tumors in rats; Group 1	OECD, 2020; Kirkland et al., 2016
	B[a]P	50-32-8	(+)	(+) for MLA, CA, MN, pig-a, comet, HPRT, UDS	(+) for comet, MN, pig-a, TG	(+) for liver, lung tumor, etc.; Group 1	Le Hegarat et al., 2010; Kirkland et al., 2016; Shah et al., 2016, 2018; Graupner et al., 2014; Guo et al., 2020; Wang et al., 2018; Dertinger et al., 2019
	CPA	6055-19-2	(+)	(+) for MLA, CA, MN	(+) for CA, MN, pig-a, TG, comet	(+) for liver, lung, skin tumor, etc.; Group 1	Yusuf et al., 2000; Kirkland et al., 2016; Seo et al., 2019, 2020; Le Hegarat et al., 2010, 2014; Bhalli et al., 2013; Dertinger et al., 2012, 2019
	DMBA	57-97-6	(+)	(+) for MLA, CA, MN, comet, UDS	(+) for MN and pig-a in blood, comet in liver, CA in BM, TG	(+) for mammary gland, liver, skin tumor, etc.	Le Hegarat et al., 2014; Kirkland et al., 2016; Shi et al., 2011
	DMNA	62-75-9	(+)	(+) for MLA, CA, MN, HPRT, comet, UDS	(+) for MN and comet in liver, UDS, TG; generally (–) for MN in BM	(+) for liver, lung and kidney tumors; Group 2A	Kirkland et al., 2016; Seo et al., 2019
	IQ	76180-96-6	(+)	(+) for SCE, UDS, MN; (+/–) for CA and comet;	(+) for CA in liver, comet, TG; (–) for MN, SCE and for CA in BM	(+) for tumors in multiple organs; Group 2A	Kirkland et al., 2016; Le Hegarat et al., 2010
	PhIP	105650-23-5	(+)	(+) for CA, MN, comet, HPRT, UDS	(+) for MN, UDS, comet, TG; (–) for CA	(+) mainly for hematopoetic tumors, also GI and prostate tumors; Group 2B	Kirkland et al., 2016; Shah et al., 2018

Group	Chemical	CAS#	Ames	Genotoxicity assay findings		Carcinogenicity[a]	References
				In vitro	*In vivo*		
In vitro (+) but *in vivo* (–), and Ames (+)	Styrene	100-42-5	(+/–)	(+) for CA, SCE, MLA, comet	(+/–) for comet, MN, CA, SCE	(+) for lung, liver, mammary gland tumors; Group 2A	Moore et al., 2019; IARC, 2019b
	3-MCPD	96-24-2	(+)	(+) for comet	(–) for pig-a, UDS, MN, comet, gpt, Spi$^-$ mutations	(+) for renal tubule tumor, Group 2B	IARC, 2013; Onami et al., 2014; Ozcagli et al., 2016
	DFPBA	156545-07-2	(+)	(+) for MLA, comet, MN	(–) for pig-a, MN, comet	No data available	Masuda-Herrera et al., 2019
	EDAC	25952-53-8	(+)	(+) for MLA, MN	(–) for pig-a, MN, comet in liver	No data available	Kirkland et al., 2019; ECHA, 2021; Custer et al., 2015
	HOPO	13161-30-3	(+), E	(+) for MN	(–) for pig-a, MN, comet	No data available	Dobo et al., 2018, 2019; Custer et al., 2015
	PBA	98-80-6	(+)	No data available	(–) for pig-a, MN, comet	No data available	Masuda-Herrera et al., 2019
In vitro (+) but *in vivo* (–), and Ames (–)	4-Nitrophenol	100-02-7	(–)	(+) for CA with S9; (–) for SCE, comet, HPRT; (+/–) for MN; I for MLA	(–) for MN	(–) in mice dermal study	Fowler et al., 2012; Eichenbaum et al., 2009; Hartmann and Speit, 1997; Hu et al., 2009; NTP, 1993
	Ethyl acrylate	140-88-5	(–)	(+) for MLA, CA; (+/–) for MN	(+/–) for MN; (–) for SCE, CA, comet, gpt and Spi$^-$ mutations	(+) for forestomach tumor in rats and mice, Group 2B	Ellis-Hutchings et al., 2018; Fowler et al., 2012; IARC, 2019a; Przybojewska et al., 1984
	Phthalic anhydride	85-44-9	(–)	(+) for MLA, comet; (–) for SCE, γH2AX; (+/–) for MN, CA	No data available	(–) in rats and mice	NTP, 2022c; Fowler et al., 2012; Smart et al., 2011; Elia et al., 1994
	Sodium xylene-sulfonate	1300-72-7	(–)	(+) for SCE; (–) for CA; (+/–) for MN; E for MLA	No data available	(–) in rats and mice dermal studies	Fowler et al., 2012; Kirkland et al., 2016; NTP, 1998
	TBHQ	1948-33-0	(–)	(+) for MLA, CA, DNA damage; (–) for HPRT and lacZ mutations; (+/–) for MN;	Borderline (+) for comet in liver; (–) for MN, CA	(–) in rats and mice	Fowler et al., 2012; Kirkland et al., 2016
In vitro (–) but *in vivo* (+)	1,4-Dioxane	123-91-1	(–)	(–) for CA, SCE, MN, MLA	(+) for MN in liver and TG; (–) for MN and pig-a in blood	(+) in rats and mice; Group 2B	Gi et al., 2018; IARC, 1999; Itoh and Hattori, 2019; Morita and Hayashi, 1998; NTP, 2022b

Group	Chemical	CAS#	Ames	Genotoxicity assay findings		Carcinogenicity[a]	References
				In vitro	*In vivo*		
	Dicyclanil	112636-83-6	(–)	(–) for CA, USD, HPRT	(+) for liver mutation, (–) for MN, comet, HPRT	(+) for liver tumor in mice	Nohmi, 2018; Umemura et al., 2007; WHO, 2021
	DMTP	120-61-6	(–)	(–) for CA, USD, CA, MN, DNA single-strand break	(+/–) for MN in BM; E for CA and SCE	(–) in rats, E in male mice	Monarca et al., 1991; Goncharova et al., 1988; Shelby et al., 1993; NTP, 2022a
	Estragole	140-67-0	(–)	(+) for MN in HepG2-CYP1A2 cells, UDS, DNA adduct; (+/–) for comet	(+) for gpt mutation, comet, DNA adduct; (–) for MN	(+) for liver tumor in mice	Nohmi, 2018; Morita et al., 2016; Ding et al., 2015; Martins et al., 2012; Schulte-Hubbert et al., 2020; Muller et al., 1994; Villarini et al., 2014
	LMG	129-73-7	(–)	(–) for comet, HPRT	(+) for liver cell mutation, DNA adduct, (–) for HPRT mutation, (+/–) for MN	(+) in rats and mice	Nohmi, 2018; Mittelstaedt et al., 2004; Culp, 2004

[a]Groups were classified by International Agency for Research on Cancer (IARC) Monographs on the identification of carcinogenic hazards to humans, Volumes 1-125 (https://monographs.iarc.who.int/list-of-classifications). +/–, both positive and negative results were reported.

BM, bone marrow; CA, chromosome aberration; E, equivocal; GI, gastrointestinal; HPRT, hypoxanthine-guanine phosphoribosyltransferase; I, inconclusive; MLA, mouse lymphoma assay; MN, micronucleus; pig-a, phosphatidylinositol glycan class A; SCE, sister chromatid exchange; TG, transgenic mutation; UDS, unscheduled DNA synthesis.

Chemicals: 2-AAF, 2-acetylaminofluorene; 2,4-DAT, 2,4-diaminotoluene; 3-MCPD, 3-chloro-1,2-propanediol; 4-NQO, 4-nitroquinoline1-oxide; AFB1, aflatoxin B1; B[a]P, benzo[a]pyrene; $CdCl_2$, cadmium chloride; CPA, cyclophosphamide; DFPBA, 3,5-difluorophenylboronic acid; DMBA, 7,12-dimethylbenzanthracene; DMNA, dimethylnitrosamine; DMTP, dimethyl terephthalate; EDAC, 1-(3-dimethylaminopropyl)-N'-ethylcarbodiimide hydrochloride; ENU, N-ethyl-N-nitrosourea; HOPO, 2-pyridinol 1-oxide; HQ, hydroquinone; IQ, 2-amino-3-methyl-3H-imidazo[4,5-f]quinoline; LMG, leucomalachite green; MMS, methyl methanesulfonate; PBA, phenylboronic acid; PhIP, 2-amino-1-methyl-6-phenylimidazo(4,5-b) pyridine; TBHQ, tertiary-butylhydroquinone

Briefly, 0.65-0.7 million undifferentiated HepaRG cells were seeded in a 100-mm tissue culture dish and cultured in 10 mL growth medium for 14 days. The cells were then differentiated in 10 mL differentiation medium for an additional 14 days. The culture medium was renewed every 2-3 days. Undifferentiated proliferative HepaRG cells were passaged every 2 weeks using TrypLE™ Express (Thermo Fisher) and the cells were passaged no more than 5 times. Absence of mycoplasma contamination in differentiated HepaRG cells was confirmed using the LookOut Mycoplasma PCR Detection Kit (Sigma-Aldrich).

2.3 Formation of 3D spheroids

Fully differentiated HepaRG cells were dissociated from tissue culture dishes using TrypLE™ Express. Following centrifugation at 300 × g for 5 min, the cells were resuspended in fresh differentiation medium and passed through a 40-µm nylon mesh cell strainer (Corning Inc., Corning, NY, USA) to minimize cell aggregation. Then cells at varying densities (5K (5,000), 10K, or 20K cells) were plated into each well of 96- or 384-well ULA round-bottom plates (Corning) in 100 µL or 50 µL medium, respectively. The culture medium was refreshed every 2-3 days by replacing half of the medium with fresh medium using VIAFLO 96/384 electronic pipettes (INTEGRA Biosciences, Hudson, NH, USA). The spheroids were incubated at 37°C in a humidified atmosphere with 5% CO_2 and maintained for up to 30 days. Images of HepaRG spheroids were acquired by a Leica DMI4000B light microscope on Days 3, 6, 10, 20, and 30 after seeding, and the diameters of spheroids were measured using the Leica Application Suite software (Leica Microsystems, Wetzlar, Germany).

2.4 Characterization of 3D spheroids

Albumin secretion

Twenty-four hours after differentiation medium was refreshed on Days 10, 20, and 30, 100 µL of culture medium was collected into a 96-well plate for the analysis of albumin secretion. The albu-

min concentration in the supernatant was determined using the Human Serum Albumin DuoSet Enzyme-linked Immunosorbent Assay (ELISA) Kit (R&D Systems, Minneapolis, MN, USA). Spheroids were lysed with RIPA buffer (Thermo Fisher), and protein concentrations were determined using the Pierce BCA Protein Assay Kit (Thermo Fisher). The albumin levels were presented as ng/mg protein.

Histology and immunohistochemistry

HepaRG spheroids were collected and fixed in 4% paraformaldehyde in Dulbecco's phosphate-buffered saline (DPBS) at 4°C overnight on Days 10, 20, and 30. Fixed spheroids were suspended in liquid HistoGel (Thermo Fisher) and solidified at 4°C overnight. The solidified gel was gently pushed into a biopsy cassette, and the HistoGel-containing HepaRG spheroids were embedded in Formula R® paraffin embedding medium (Leica Biosystems, Wetzlar, Germany). Paraffin-embedded blocks were sectioned at approximately 5 µm thickness, and the sections were mounted on positively charged glass slides. Spheroid sections were deparaffinized in xylene and hydrated in a graded series of ethanol solutions. One set of sections was stained with hematoxylin and eosin (H&E), the other three sets were immunohistochemically stained for cytokeratin 19 (CK19, biliary epithelial cells marker), Ki67 (proliferation marker), and multidrug resistance-associated protein 2 (MRP2, a canalicular multispecific organic anion transporter). Spheroid sections were incubated with the following primary antibodies: mouse monoclonal anti-CK19 (MAB3238, Sigma-Aldrich), rabbit monoclonal Ki67 (RM-9106, Thermo Fisher), and mouse monoclonal anti-MRP2 (ab3373, Abcam, Waltham, MA, USA) at dilutions of 1:200 (CK19) and 1:100 (Ki67 and MRP2) for 1 h. Slides then were incubated with the appropriate secondary antibodies: rat anti-mouse IgG-Cy3 or donkey anti-rabbit IgG $F(ab')_2$ fragment-Cy3 (415-165-166 or 711-166-152, respectively, Jackson ImmunoResearch Laboratories, West Grove, PA, USA). The sections were counterstained and mounted with Vectashield/DAPI (Vector Laboratories, Inc., Burlingame, CA, USA). Stained sections were examined, and microphotographs were taken with a Nikon Eclipse Ni-E upright motorized microscope (Tokyo, Japan).

CYP450 enzyme activities

The basal activities of CYP450 enzymes in HepaRG spheroids were measured by incubating the spheroids with seven CYP substrates as described previously with minor modifications (Seo et al., 2019, 2020). Briefly, spheroids were incubated for 2 h with 100 µL differentiation medium containing 40 µM chlorzoxazone (CYP2E1) or substrate cocktails of 100 µM phenacetin (CYP1A2), 100 µM bupropion (CYP2B6), 20 µM diclofenac (CYP2C9), 20 µM omeprazole (CYP2C19), 20 µM dextromethorphan (CYP2D6), and 50 µM midazolam (CYP3A4) at 37°C in a humidified atmosphere with 5% CO_2. At the end of incubation, the supernatants were collected, and the protein was removed by adding twice the volume of acetonitrile containing 100 ng/mL of Bup-OH-D6 (internal standard). The individual metabolites released into the medium were quantified by high-performance liquid chromatography-tandem mass spectrometry (HPLC-MS/MS) using a Shimadzu 20A ultra-fast liquid chromatograph (UFLC) system coupled with an AB SCIEX 3200 QTRAP mass spectrometer (SCIEX LLC, Framingham, MA, USA). Chromatographic separation was performed using an Atlantis T3 C18 column (4.6 × 150 mm, 5 µm) with an Atlantis T3 VanGuard pre-column (3.9 × 5 mm, 5 µm) (Waters Corporation, Milford, MA, USA) maintained at 40°C. Samples (injection volume of 4 µL) were separated at a flow rate of 0.5 mL/min using a gradient mobile phase containing water (Solvent A) and acetonitrile (Solvent B), both containing 0.1% formic acid. The gradient was as follows: 0-0.2 min, 5% Solvent B; 0.2-10 min, 5-95% Solvent B; 10-10.5 min, 95-5% Solvent B; 10.5-15 min, 5% Solvent B for column re-equilibration. The mass spectrometer with electrospray ionization (ESI) source was operated in the negative ion mode for Chlorz-OH (CYP2E1) and in the positive ion mode for the other six metabolites. Multiple reaction monitoring (MRM) was used for quantitation with the following ion transitions: *m/z* 152.2-110.1 for APAP (CYP1A2), *m/z* 256.1-238.2 for Bup-OH (CYP2B6), *m/z* 312.1-230.0 for Dic-OH (CYP2C9), *m/z* 362.2-214.2 for OPZ-OH (CYP2C19), *m/z* 258.2-157.2 for Dex (CYP2D6), *m/z* 184.0-120.0 for Chlorz-OH (CYP2E1), and *m/z* 342.1-203.1 for Mid-OH (CYP3A4). Following a 2-h exposure to CYP substrates, the spheroids were lysed with RIPA buffer, and the protein concentrations were measured using the Pierce BCA Protein Assay Kit. Final CYP450 activities were expressed as pmol metabolite/min/mg protein. The activities of CYP450 in PHHs (Lot# HH1085, In Vitro ADMET Laboratories, Columbia, MD, USA) were obtained from our previous study (Seo et al., 2020).

Gene expression of phase I and phase II enzymes

The basal gene expression levels of 14 phase I and 5 phase II enzymes were measured using quantitative real-time PCR (qPCR) at the mRNA level. Total RNA was extracted from 2D cultured cells at Day 3, 5K 3D spheroids (spheroids containing 5K HepaRG cells) at Day 10 and cryopreserved PHHs (Lot# HH1085) using the RNeasy Mini kit (Qiagen, Valencia, CA, USA). RNA concentration and quality were measured using a NanoDrop 8000 spectrophotometer (Thermo Fisher). cDNA was synthesized from 1 µg of total RNA using the High-Capacity cDNA Reverse Transcription kit (Applied Biosystems, Foster City, CA, USA). qPCR was performed using the FastStart Universal Probe Master (Rox) (Roche Applied Science, Indianapolis, IN, USA) with the following TaqMan™ probes (Applied Biosystems): CYP1A1 (Hs01054796_g1), CYP1A2 (Hs00167927_m1), CYP1B1 (Hs00164383_m1), CYP2A6 (Hs00868409_s1), CYP2A13 (Hs00711162_s1), CYP2B6 (Hs03044634_m1), CYP2C8 (Hs00946140_g1), CYP2C9 (Hs00426397_m1), CYP2C19 (Hs00426380_m1), CYP2D6 (Hs04931916_gH), CYP2E1 (Hs00559367_m1), CYP3A4 (Hs00604506_m1), CYP3A5 (Hs00241417_m1), CYP3A7 (Hs00426361_m1), N-acetyltransferase 1 (NAT1; Hs00265080_s1), sulfotransferase 1A1 (SULT1A1; Hs00738644_m1), SULT2A1 (Hs00234219_m1), UDP-glucuronosyltransferase 1A1 (UGT1A1; Hs02511055_s1), UGT1A6 (Hs01592477_m1), and glyceraldehyde 3-phosphate dehydrogenase (GAPDH;

Hs02758991_g1). Triplicates of 20 µL for each sample were amplified in 96-well plates using the ViiA™ 7 Real-Time PCR system (Applied Biosystems) under the following thermocycling conditions: 1 cycle at 50°C for 2 min, 1 cycle at 95°C for 10 min, and 40 cycles of 95°C for 15 sec, and 60°C for 1 min. The relative mRNA level (the fold-change of target gene expression) was calculated using the $2^{-\Delta\Delta Ct}$ method with normalization to GAPDH.

2.5 Chemical treatment

For 3D cultures, fully differentiated HepaRG cells were plated into 384-well ULA plates at cell densities of 5K-10K cells per well in 50 µL of William's E differentiation medium. Ten days after seeding, 5-7 spheroids were transferred into each well of a 96-well round-bottom plate (TPP, Switzerland). For 2D cultures, fully differentiated HepaRG cells were seeded into a 96-well flat bottom plate at a density of 5×10^4 cells/well. Both 3D spheroids and 2D HepaRG cells were subsequently exposed to various concentrations of test articles (Tab. 1).

Stock solutions were prepared by dissolving cadmium chloride ($CdCl_2$) and dimethylnitrosamine (DMNA) in deionized water, cisplatin in 0.9% NaCl (Sigma-Aldrich), and the other 31 chemicals in DMSO (Sigma-Aldrich), and stored at -20°C. Cisplatin, *N*-ethyl-*N*-nitrosourea (ENU), hydroquinone (HQ), and tertiary-butylhydroquinone (TBHQ) were freshly prepared before each experiment. Working solutions (100 ×) were prepared by serial dilutions in differentiation medium. The final concentration of DMSO in cell culture experiments never exceeded 1%. HepaRG in 2D and 3D cultures were treated with various concentrations of the test chemicals in a total volume of 100 µL for 24 h at 37°C. The experiments were repeated independently at least three times for each chemical.

2.6 Cytotoxicity assay

Cytotoxicity was evaluated by ATP assay using CellTiter-Glo® luminescent cell viability assay kit (Promega). Following 24-h treatment, the ATP reagent was added into each well at a ratio of 1:10 and was incubated for 10 min at room temperature. The luminescence from the luciferase reaction was recorded with a Cytation 5 Cell Imaging Multi-Mode Reader (BioTek, Winooski, VT, USA). The relative cell viability was expressed as the percentage of intensity of the treated cells compared to the cells treated with respective vehicle controls.

2.7 Alkaline CometChip assay

Following 24-h treatment, DNA damage was evaluated by CometChip assay as described previously with minor modifications for 3D cultures (Seo et al., 2019). Briefly, 96-well plates containing 3D spheroids were centrifuged at 300 × g for 5 min, and differentiation medium was removed carefully. After a short wash with DPBS, 35 µL of TrypLE™ Express was added into each well of the plates and incubated for 15 min at 37°C. Subsequently, spheroids were dissociated into single cell suspensions by gentle pipetting, followed by addition of 100 µL differentiation medium to stop the reaction. Next, the cells were transferred into each well of a 96-well CometChip (Trevigen, Gaithersburg, MD, USA), and the comet assay was conducted as described previously (Seo et al., 2020). Comet images were acquired automatically using a Cytation 5 Cell Imaging Multi-Mode Reader (BioTek) and analyzed using Trevigen Comet Analysis Software to calculate the percentage of DNA in the tail (% tail DNA). DNA damage responses also were expressed as the relative ratio of DNA damage (fold-change) compared to their respective controls (Fig. S1[1]).

2.8 Quantification of DNA damage dose-response data

BMD analysis was performed using PROAST software (version 70.1). DNA damage dose-response data were analyzed using both exponential and Hill models that are recommended by the European Food Safety Authority (EFSA) for the analysis of continuous data (EFSA et al., 2017). The critical effect size (CES) of 0.5, indicating a 50% increase (BMD_{50}) in % tail DNA over the vehicle control response, was chosen for the *in vitro* comet assay (Seo et al., 2021). The BMD_{50} and its BMDU and BMDL were calculated simultaneously for each data set. Uncertainty of the BMD estimates, indicated by the BMDU/BMDL ratio, was used to evaluate the statistical quality of the data (Slob, 2017).

2.9 Statistical analysis

Data are presented as the mean ± SD from at least three independent experiments. The statistical significance was evaluated by one-way analysis of variance (ANOVA) followed by Holm-Sidak test for albumin secretion, CYP450 activity, and gene expression data of phase I and phase II enzymes (SigmaPlot 13.0, Systat Software, San Jose, CA, USA). ANOVA followed by Dunnett's test was used for comparing the CometChip data between treatment groups and the vehicle control group. A value of $p < 0.05$ was considered statistically significant.

3 Results

3.1 HepaRG spheroid formation and size

HepaRG cells were grown to confluence in complete growth medium for 14 days and then differentiated with complete differentiation medium for another 14 days. Two morphologically distinct cell populations were observed, i.e., clustered granular hepatocyte-like cells surrounded by relatively clear biliary epithelial-like cells (Fig. 1A). After seeding in 96- or 384-well ULA plates, differentiated HepaRG cells, at three different densities (5K, 10K, and 20K/well), aggregated into spheroids without any supporting exogenous extracellular matrix after 3 days of culture (Fig. 1B). At Day 3, the diameters of 5K, 10K, and 20K spheroids averaged 369.4 ± 29.9 µm, 537.5 ± 31.0 µm, and 658.5 ± 56.2 µm, respectively. The spheroids became more compact over a period of 30 days, along with 15.8-31.6% reduction in size. At Day 30, 5K, 10K, and 20K spheroids were sized 310.9 ± 14.5 µm, 396.7 ± 10.3 µm, 450.2 ± 17.5 µm, respectively.

[1] doi:10.14573/altex.2201121s

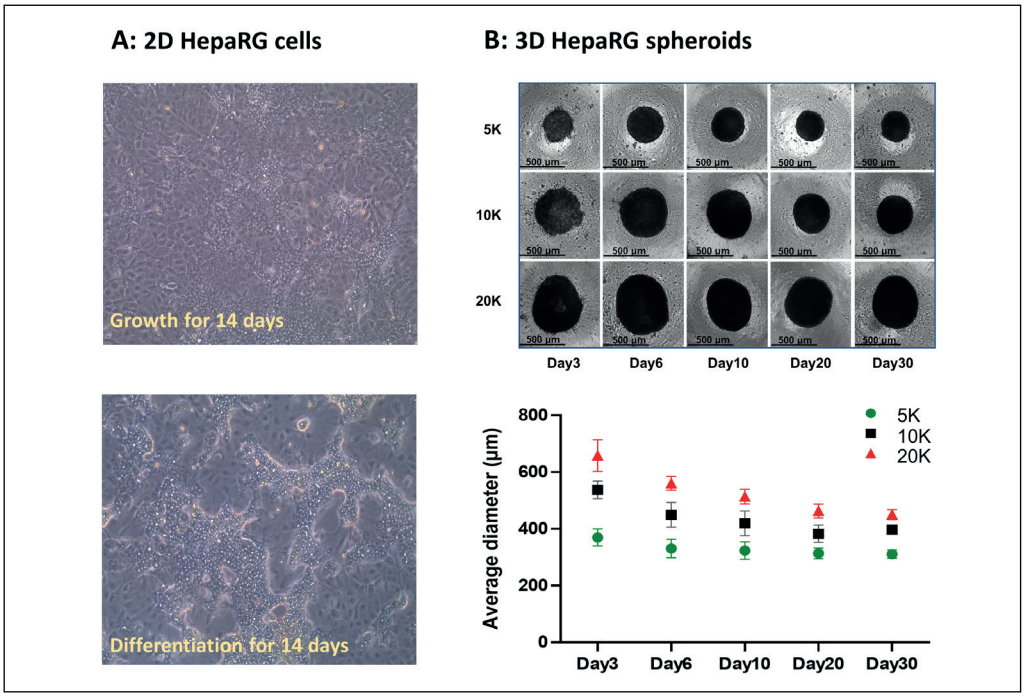

Fig 1: 2D and 3D HepaRG cultures
(A) Cell morphology of 2D HepaRG cells cultured in growth medium for 14 days and in differentiation medium for an additional 14 days (200 × magnification). (B) HepaRG cells were seeded at 5,000, 10,000, and 20,000 (5K, 10K, and 20K) per well in ultra-low attachment (ULA) plates and cultured for up to 30 days. The morphology and size of 3D spheroids were measured at Days 3, 6, 10, 20, and 30 using a light microscope. Scale bar = 500 μm.

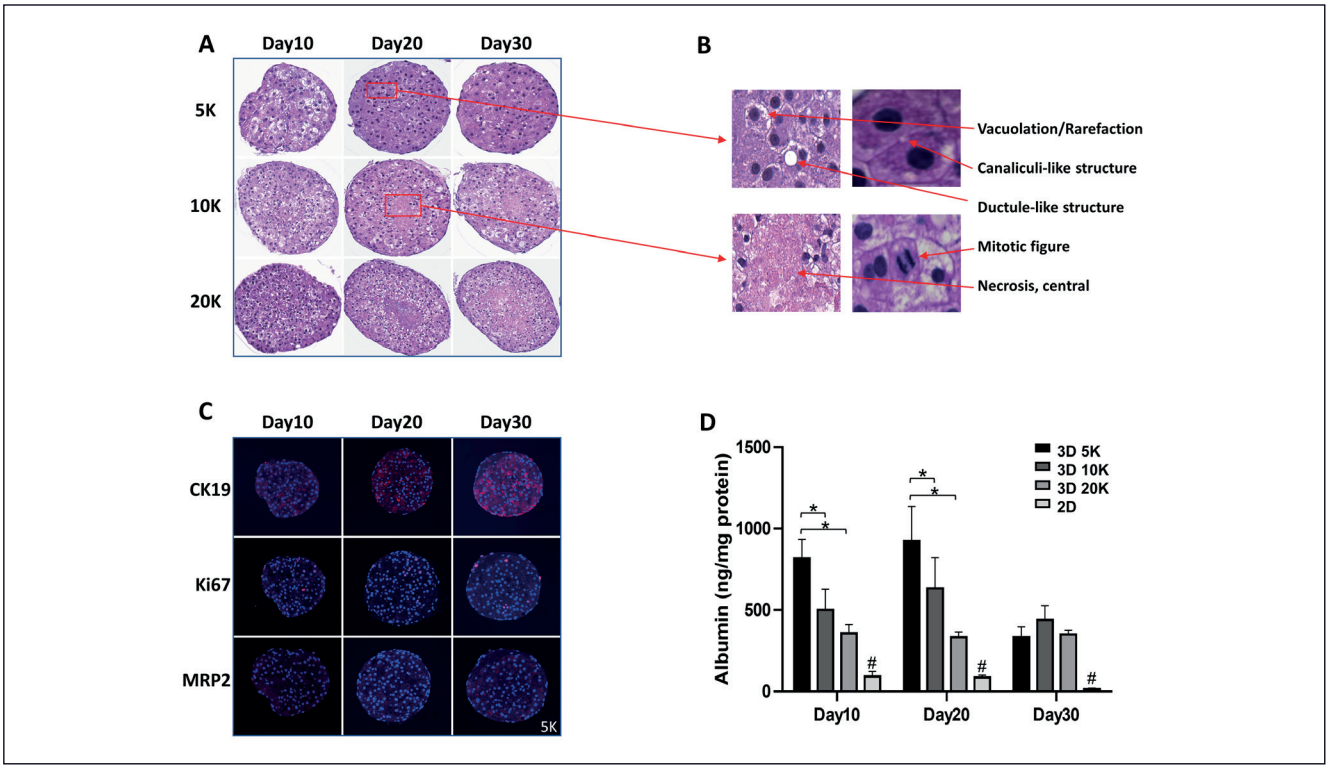

Fig. 2: Characterization of HepaRG spheroids
(A) H&E staining of 5K, 10K, and 20K spheroids. (B) Representative images of vacuolation, canaliculi-like and ductule-like structures, necrosis, and mitotic figure visible in stained spheroids. (C) Immunofluorescent staining with the biliary epithelial cell marker CK19, proliferation marker Ki67, and canalicular marker MRP2 (5K spheroids data shown; see Fig. S1[1] for 10K and 20K spheroids). (D) Albumin secretion was measured by ELISA and expressed as ng/mg protein. The data are presented as the mean ± SD (n ≥ 3). Significance was determined by one-way ANOVA followed by Holm-Sidak test (*$p < 0.05$ for comparison of 5K, 10K, and 20K spheroids, $^{\#}p < 0.05$ for 2D HepaRG cells vs 5K or 10K spheroids). H&E, hematoxylin and eosin; CK19, cytokeratin 19; MRP2, multidrug resistance-associated protein 2.

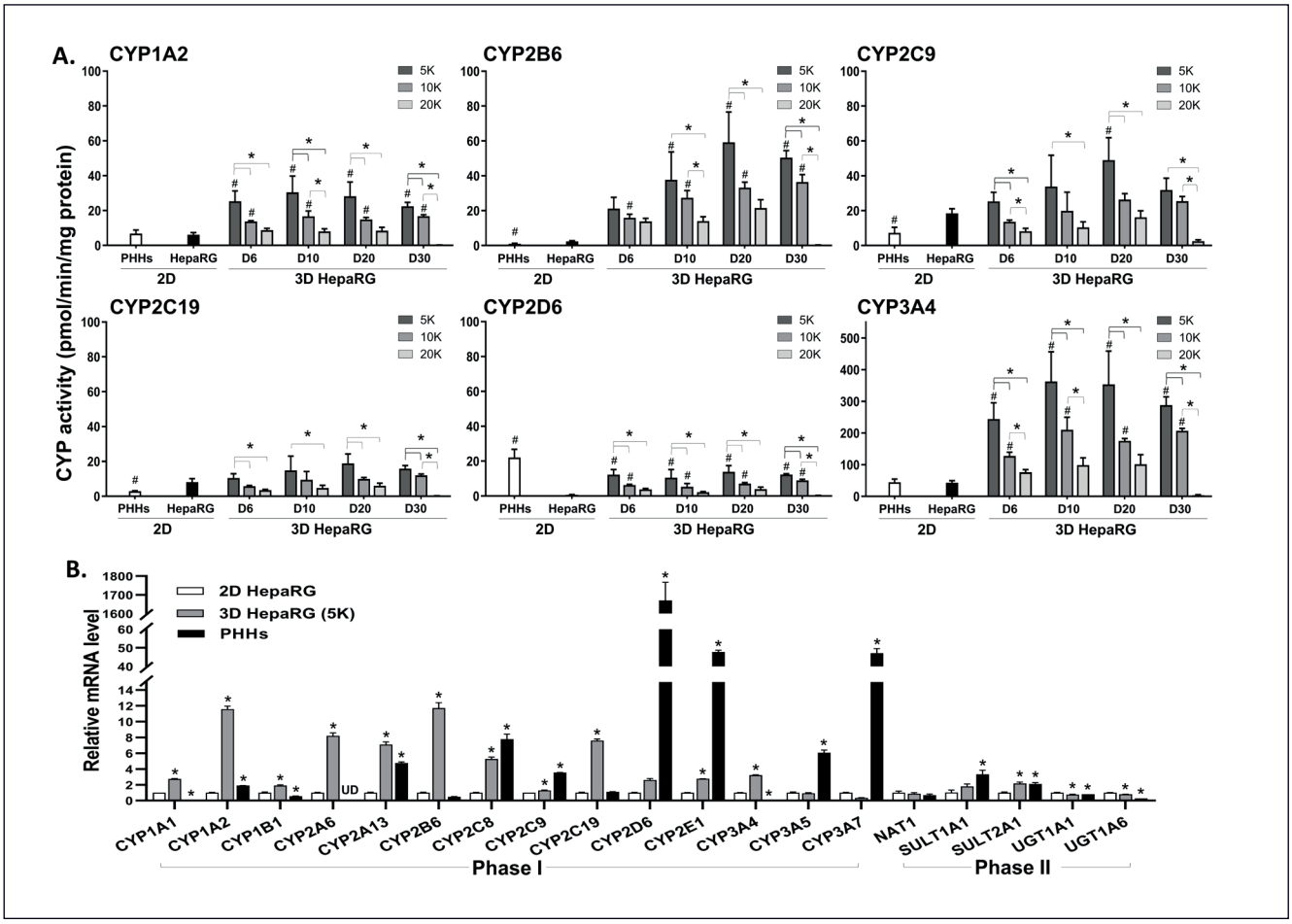

Fig. 3: Cytochrome P450 enzyme (CYP450) activity and gene expression of phase I and phase II enzymes in primary human hepatocytes (PHHs), 2D, and 3D HepaRG cultures

(A) Six major CYP450 activities (CYP1A2, 2B6, 2C9, 2C19, 2D6, and 3A4) were measured in PHHs, 2D HepaRG cells, and 3D HepaRG (5K, 10K, and 20K) spheroids at Days 10, 20, and 30 after seeding. CYP450 activities are expressed as pmol/min/mg protein, and the data are presented as the mean ± SD (n ≥ 3). (B) Relative mRNA expression was measured by quantitative real-time PCR (qPCR). Total RNA was extracted from PHHs, 2D HepaRG cells, and 5K spheroids for cDNA synthesis. qPCR data was normalized to GAPDH expression. The data are presented as the mean ± SD (n ≥ 3). Significant difference was determined by one-way ANOVA followed by Holm-Sidak test (*$p < 0.05$ for comparison of 5K, 10K, and 20K spheroids, $^{\#}p < 0.05$ for 2D HepaRG cells vs 5K or 10K spheroids). UD, undetermined; NAT, *N*-acetyltransferase; SULT, sulfotransferase; UGT, UDP-glucuronosyltransferase; and GAPDH, glyceraldehyde 3-phosphate dehydrogenase.

3.2 Histological and immunohistochemical analyses of HepaRG spheroids

Morphological features of 5K, 10K, and 20K spheroids at Days 10, 20, and 30 were assessed with H&E staining (Fig. 2A). The spheroids consisted of large, polygonal cells with round to oval single nuclei (rarely binucleated), 1-2 nucleoli, clear and/or granular cytoplasm with vacuolation and/or rarefaction, and low nuclear to cytoplasmic ratio. Most cells in spheroids morphologically resembled hepatocytes and occasionally appeared to form canaliculi-like structures. There were also rare ductule-like structures that appeared to have a central lumen lined with cuboidal cells (Fig. 2B). Mitotic figures were seen occasionally. Viable cells were observed at the centers of the majority of 5K spheroids, whereas higher incidences of necrotic cores were observed in 10K and 20K spheroids at Days 20 and 30 (Fig. 2A).

Immunofluorescent staining showed expression of the biliary marker CK19 protein in the spheroids for at least 30 days of cultivation, with expressions enhanced over time (Fig. 2C, Fig. S2[1]). Ki67 protein was detected in the spheroids, indicating cellular proliferation potential. During 30 days of culture, 5K and 10K spheroids expressed relatively higher levels of Ki67 protein compared to 20K spheroids. The expression of MRP2 protein also was confirmed on the canalicular membrane of cells in the spheroids, indicating that bile canaliculi structures were formed in 3D HepaRG spheroids (Fig. 2C).

3.3 Albumin secretion in 2D and 3D HepaRG cultures

Albumin secreted into culture medium within 24 h after seeding was measured in both 2D and 3D cultures (Fig. 2D). Sig-

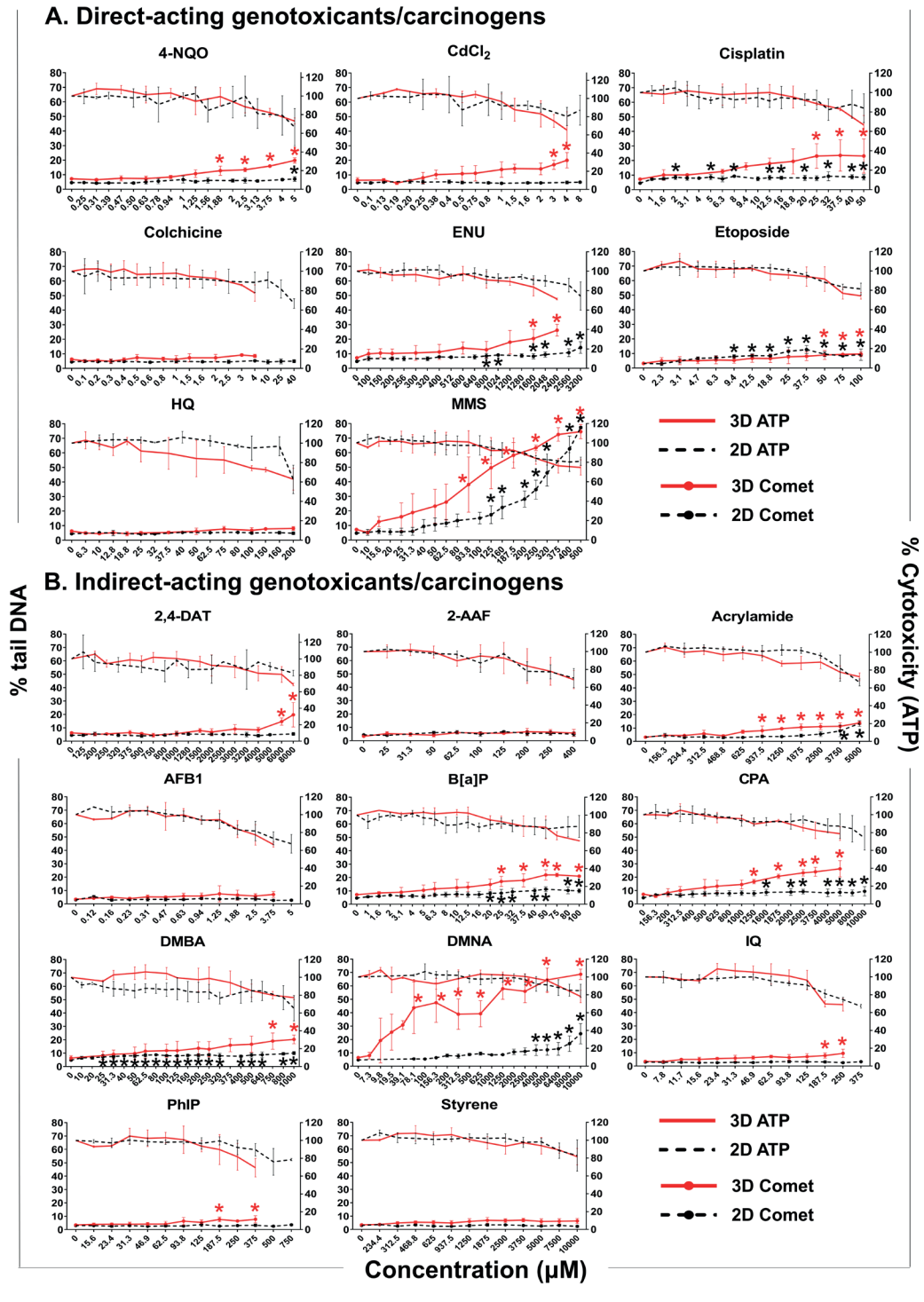

Fig. 4: DNA damage and cytotoxicity of 19 genotoxicants/carcinogens in 2D and 3D HepaRG cultures

2D and 3D HepaRG cultures were exposed to 8 direct-acting (A) and 11 indirect-acting genotoxicants/carcinogens (B) for 24 h. Part of the DNA damage and cytotoxicity data in 2D HepaRG cells was obtained from our previous study (Seo et al., 2019). The relative cell viability (% of control, indicating cytotoxicity) was measured by ATP assay (right y-axis and top two lines). DNA damage (% tail DNA; left y-axis and bottom two lines) was detected using the CometChip assay. The red lines and black dotted lines represent the results of 3D and 2D HepaRG cultures, respectively. The data are expressed as the mean ± SD (n ≥ 3). Significance was determined by one-way ANOVA followed by Dunnett's test (*$p < 0.05$ vs vehicle control). See Table 1 for abbreviations of the compounds tested.

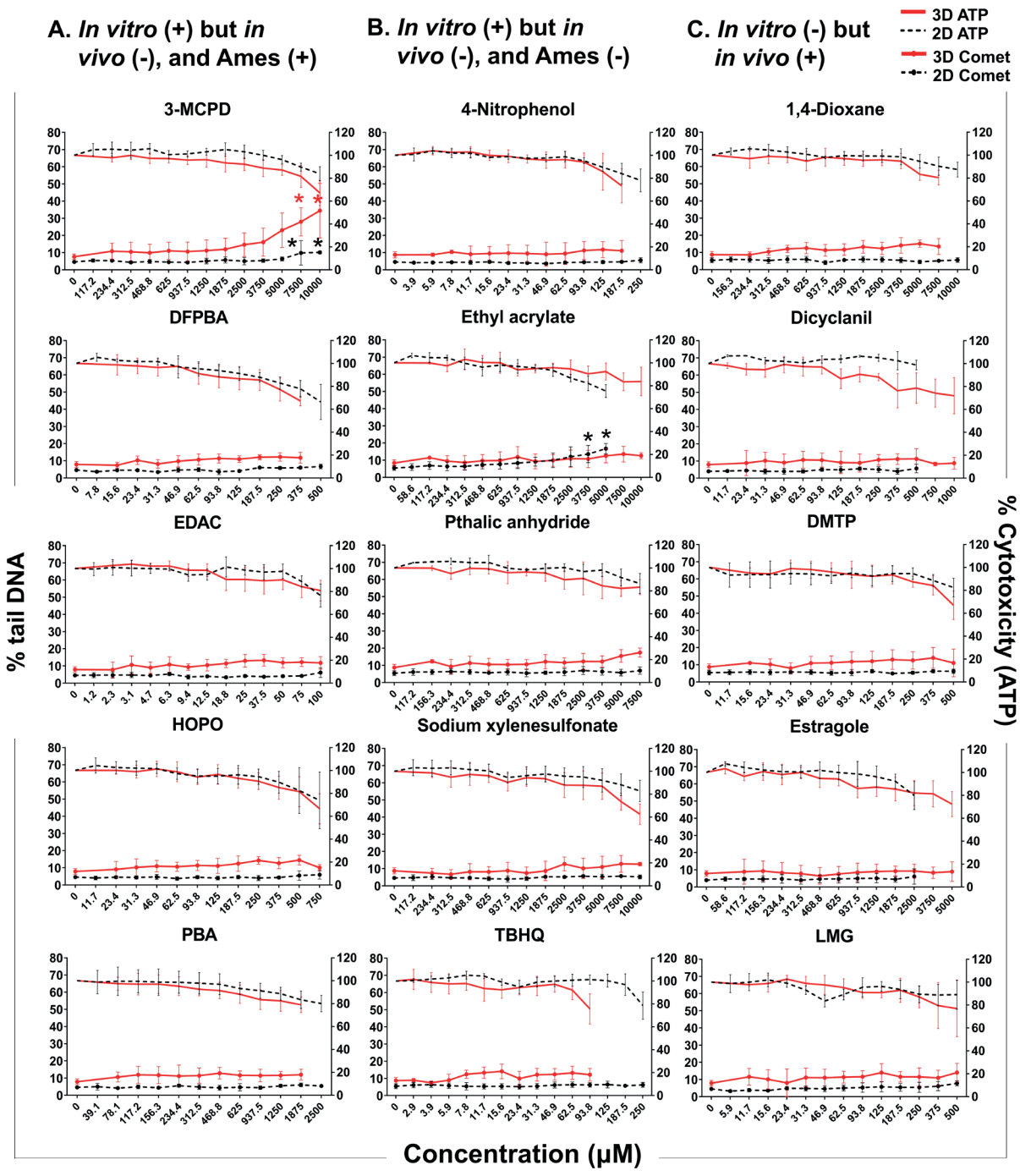

Fig. 5: DNA damage and cytotoxicity of 15 compounds that show different genotoxic responses *in vitro* and *in vivo* in 2D and 3D HepaRG cultures

2D and 3D HepaRG cultures were exposed to 15 compounds including five *in vitro* (+) but *in vivo* (-) and Ames (+) compounds (A); five *in vitro* (+) but *in vivo* (-) and Ames (-) compounds (B); and five *in vitro* (-) but *in vivo* (+) compounds for 24 h. The relative cell viability (% of control, indicating cytotoxicity) was measured by ATP assay (right y-axis and top two lines). DNA damage (% tail DNA; left y-axis and bottom two lines) was detected using the CometChip assay. The red lines and black dotted lines represent the results of 3D and 2D HepaRG cultures, respectively. The data are expressed as the mean ± SD (n ≥ 3). Significance was determined by one-way ANOVA followed by Dunnett's test (*$p < 0.05$ vs vehicle control). See Tab. 1 for abbreviations of the compounds tested.

nificantly higher albumin secretion (ng/mg protein) was shown in 3D spheroids compared to 2D HepaRG cells over an incubation period of 30 days. When compared to 2D cultures, the albumin level of 5K spheroids increased by 9.0-, 10.8-, and 23.4-fold with values of 818.2, 922.6, and 334.9 ng/mg protein (vs 91.3, 85.2, and 14.3 ng/mg protein in 2D) at Days 10, 20, and 30, respectively. Additionally, 5K spheroids produced 1.5-1.6-fold and 2.3-2.9-fold higher albumin levels than 10K and 20K spheroids at Days 10 and 20, respectively. At Day 30, the albumin secretion in 5K spheroids declined to levels equivalent to those in 10K and 20K spheroids.

3.4 CYP450 enzyme activities in PHHs, 2D, and 3D HepaRG cultures

The activities of seven major CYP450 (CYP1A2, 2B6, 2C9, 2C19, 2D6, 2E1, and 3A4) enzymes were measured by determining the formation of metabolites released into the medium via HPLC-MS/MS (Fig. 3A). The activity of CYP2E1 in PHHs was 1.6 pmol metabolite/min/mg protein, while it was below the quantification limit in both 2D HepaRG and 5K, 10K, or 20K spheroids under our experimental conditions (data not shown in Fig. 3A). The 5K and 10K spheroids maintained high activities for the other six CYPs over a culture period of 30 days, while a sharp decline was observed in 20K spheroids at Day 30. The 5K spheroids showed the highest CYP450 activities across the six CYPs, followed by 10K and 20K spheroids (5K > 10K > 20K). Specifically, the CYP activities in 5K spheroids were 1.3-2.0-fold and 1.5-3.8-fold higher than those in 10K and 20K spheroids, respectively, while the CYP activities in 10K spheroids were consistently higher (1.6-2.4-fold) than those in 20K spheroids.

When compared to 2D HepaRG cells, 5K and 10K spheroids displayed significantly higher activities for CYP1A2 (2.2-4.9-fold), 2B6 (6.7-25.0-fold), 2D6 (7.7-20.4-fold), and 3A4 (2.9-8.3-fold) for up to 30 days. Similar or slightly higher activities were observed for CYP2C9 (0.7-2.7-fold) and 2C19 (0.7-2.3-fold) between 2D and 3D cultures. CYP2D6 activity was 32.5-fold higher in PHHs than in 2D HepaRG cells, whereas 2D HepaRG cells had 2.5-fold higher CYP2B6 and 2C9 activities compared to PHHs. There was no significant difference in CYP1A2 and 3A4 between PHHs and 2D HepaRG cells.

3.5 Gene expression of phase I and phase II enzymes in 5K spheroids

Gene expression of phase I and phase II enzymes was determined using qPCR (Fig. 3B). In agreement with increased CYP450 enzyme activities seen in 3D cultures, 5K spheroids showed significantly higher mRNA expression than 2D HepaRG cells for 12 phase I enzymes: CYP1A1 (2.7-fold), 1A2 (11.6-fold), 1B1 (1.9-fold), 2A6 (8.2-fold), 2A13 (7.1-fold), 2B6 (11.7-fold), 2C8 (5.3-fold), 2C9 (1.3-fold), 2C19 (7.6-fold), 2D6 (2.6-fold), 2E1 (2.7-fold), and 3A4 (3.2-fold). CYP3A5 and 3A7 expression did not differ significantly between 2D HepaRG cells and 5K spheroids. The gene expression of CYP1A1, 1B1, 2A6 (undetermined), and 3A4 in PHHs was significantly lower than in 2D and 3D HepaRG cultures, whereas PHHs had considerably higher levels of CYP2D6, 2E1, 3A5, and 3A7 gene expression compared to 2D and 3D HepaRG cultures. For 5 phase II enzymes, no significant changes were found for NAT1 in 5K spheroids and PHHs compared to 2D HepaRG cells. Two sulfotransferases, SULT1A1 and 2A1, were increased in 3D spheroids (1.8-2.2-fold) and PHHs (2.1-3.3-fold), whereas two UDP-glucuronosyltransferases, UGT1A1 and 1A6, were slightly lower in 3D spheroids (0.8-fold) and PHHs (0.3-0.8-fold) compared to 2D HepaRG cells.

3.6 Cytotoxicity profiles of the 34 tested compounds in 2D and 3D HepaRG cultures

Following 24-h exposure, the cytotoxicity of 34 test articles was evaluated over a wide range of concentrations by the ATP assay. Seven out of 19 genotoxicants/carcinogens ($CdCl_2$, colchicine, ENU, AFB1, CPA, IQ, and PhIP) and five out of 15 compounds that show different genotoxic responses *in vitro* and *in vivo* (3,5-difluorophenylboronic acid (DFPBA), PBA, 4-nitrophenol, TBHQ, and 1,4-dioxane) were more cytotoxic in 3D spheroids than in 2D cultures (Tab. 2, Fig. 4, 5). Other compounds induced similar cytotoxic effects between 2D and 3D cultures with one exception, ethyl acrylate, which showed higher cytotoxicity in 2D cultured cells than in 3D spheroids.

3.7 DNA damage profiles of the 34 tested compounds in 2D and 3D HepaRG cultures

To minimize false-positive genotoxicity responses in the CometChip assay, a cytotoxicity cutoff value of 70% was chosen for evaluating DNA damage responses (Koppen et al., 2017). When no cytotoxicity was observed, the highest test concentration used for subsequent testing was 10 mM, as recommended by the OECD guidance for genetic toxicology testing (OECD, 2017).

Table 2 summarizes DNA damage responses of the 34 compounds in 2D and 3D cultures. At the maximum concentration for each compound, 14 out of 19 (73.7%) genotoxicants/carcinogens induced DNA damage in 3D spheroids, while 10 out of 19 (52.6%) genotoxicants/carcinogens were positive in 2D cultured cells after a 24-h treatment. For the 8 direct-acting genotoxicants/carcinogens, $CdCl_2$ was the only compound that showed different DNA damage responses between 2D and 3D cultures, i.e., a 3.1-fold increase in DNA damage was observed in 3D spheroids, but not in 2D cultured cells (Fig. 4A, Tab. 2). Two compounds (4-nitroquinoline 1-oxide (4-NQO) and cisplatin) induced relatively higher % tail DNA in 3D spheroids than in 2D cultured cells (2.7-3.2-fold vs 1.6-1.9-fold increase over control, respectively). When the lowest effective concentrations (LECs) were compared, 4-NQO and MMS had lower LEC values in 3D spheroids compared to 2D cultured cells (1.88 vs 5 µM and 93.8 vs 125 µM, respectively). Cisplatin, ENU, and etoposide showed higher LEC values (25 vs 2 µM, 1600 vs 800 µM, and 50 vs 9.4 µM, respectively) in 3D spheroids than in 2D cells. HQ and aneugen colchicine produced negative responses in both culture models.

At the maximum concentrations, all 11 indirect-acting genotoxicants/carcinogens induced higher % tail DNA in 3D spheroids compared to 2D cultured cells (Fig. 4B, Fig. S1[1]). Five compounds, acrylamide, B[*a*]P, cyclophosphamide (CPA), 7,12-dimethylbenzanthracene (DMBA), and DMNA, induced DNA damage in both culture models, while three compounds, 2,4-diaminotoluene (2,4-DAT), IQ, and PhIP, were positive only in

Tab. 2: Comparison of DNA damage induced in 2D and 3D HepaRG cell cultures

Compound		Max conc. (μM)[a]		Cytotoxicity (%)[b]		LEC[c]		Relative ratio[d]		Outcome[e]	
		2D	3D	2D	3D	2D	3D	2D	3D	2D	3D
Genotoxicants/carcinogens											
Direct-acting genotoxicants/ carcinogens	4-NQO	5	5	33	27	5	1.88	1.6	2.7	+	++
	$CdCl_2$	8	4	13	35	-	3	1.1	3.1	-	++
	Cisplatin	50	50	16	33	2	25	1.9	3.2	+	++
	Colchicine	40	4	33	22	-	-	1.1	1.0	-	-
	ENU	3,200	2,400	26	29	800	1,600	3.0	3.6	++	++
	Etoposide	100	100	19	26	9.4	50	3.0	3.0	++	++
	HQ	200	200	37	37	-	-	1.1	1.3	-	-
	MMS	500	500	19	25	125	93.8	16.2	10.3	+++	+++
Indirect-acting genotoxicants/ carcinogens	2,4-DAT	8,000	8,000	17	31	-	6,000	1.2	3.1	-	++
	2-AAF	400	400	30	31	-	-	1.1	1.7	-	-*
	Acrylamide	5,000	5,000	34	27	3,750	937.5	4.2	4.3	++	++
	AFB1	5	3.75	33	33	-	-	0.9	2.0	-	-*
	B[*a*]P	100	100	13	29	20	25	2.2	2.9	++	++
	CPA	10,000	5,000	26	21	1,600	1,250	2.0	3.6	+	++
	DMBA	1,000	1,000	35	23	25	750	2.1	3.2	++	++
	DMNA	10,000	10,000	15	22	4,000	78.1	5.1	10.6	+++	+++
	IQ	375	250	33	31	-	187.5	1.1	2.7	-	++
	PhIP	750	375	21	31	-	187.5	0.8	2.2	-	++
	Styrene	10,000	10,000	17	18	-	-	0.8	1.8	-	-*
***Compounds that show different genotoxic responses* in vitro *and* in vivo**											
In vitro (+) but *in vivo* (-), and Ames (+)	3-MCPD	10,000	10,000	16	33	7,500	5,000	2.2	4.5	++	++
	DFPBA	500	375	34	33	-	-	1.5	1.5	-	-
	EDAC	100	100	24	19	-	-	1.3	1.5	-	-
	HOPO	750	750	26	33	-	-	1.3	1.3	-	-
	PBA	2,500	1,875	20	21	-	-	1.2	1.5	-	-
In vitro (+) but *in vivo* (-), and Ames (-)	4-Nitrophenol	250	187.5	22	27	-	-	1.2	1.3	-	-
	Ethyl acrylate	5,000	10,000	28	16	3,750	-	3.1	1.5	++	-
	Phthalic anhydride	7,500	7,500	14	17	-	-	1.3	2.0	-	-*
	Sodium xylenesulfonate	10,000	10,000	17	37	-	-	1.1	1.4	-	-
	TBHQ	250	93.8	21	33	-	-	1.1	1.4	-	-
In vitro (-) but *in vivo* (+)	1,4-Dioxane	10,000	7,500	13	20	-	-	1	1.5	-	-
	Dicyclanil	500	1,000	1	28	-	-	1.4	1.1	-	-
	DMTP	500	500	18	33	-	-	1.1	1.3	-	-
	Estragole	2,500	5,000	20	28	-	-	1.5	1.1	-	-
	LMG	500	500	11	23	-	-	1.7	1.8	-*	-*

[a] The highest concentration tested in the CometChip assay. [b] Cytotoxicity was determined using the ATP assay following a 24-h treatment. [c] LEC, the lowest effective concentration, determined by one-way ANOVA followed by Dunnett's test, is the lowest concentration that induced a significant increase in % tail DNA. [d] The relative ratio compared to the % tail DNA of the vehicle control at the concentration shown in the table. [e] The ratio ≤ 1.5-fold ($p \geq 0.05$ vs vehicle control, green color); *, 1.5 < ratio ≤ 2, but $p \geq 0.05$ (green color); +, 1.5 < ratio ≤ 2; ++, 2 < ratio ≤ 5; +++, the ratio > 5 ($p < 0.05$, red color). See Table 1 for abbreviations of the compounds tested.

3D HepaRG spheroids (Tab. 2). The relative DNA damage ratios of 2-acetylaminofluorene (2-AAF), AFB1, and styrene increased by 1.7-2.0-fold in 3D spheroids, but this was not statistically significant compared to the control group. Acrylamide, CPA, and DMNA had lower LEC values in 3D spheroids than in 2D cultures (937.5 vs 3750 µM, 1250 vs 1600 µM and 78.1 vs 4000 µM, respectively), while the LECs of B[*a*]P and DMBA were lower in 2D cultured cells than in 3D spheroids (20 vs 25 µM and 25 vs 750 µM, respectively).

For the 15 compounds that showed different genotoxic responses *in vitro* and *in vivo*, 3D and 2D cultures showed consistent positive/negative calls for all the compounds except ethyl acrylate (Fig. 5, Tab. 2). Ethyl acrylate was positive in 2D cultured cells at concentrations ≥ 3750 µM, while it did not induce significant DNA damage in 3D spheroids. 3-chloro-1,2-propanediol (3-MCPD) was the only compound that induced positive responses in both culture models, with lower LEC (5000 vs 7500 µM) and higher relative ratio observed in 3D spheroids than in 2D cultured cells (4.5-fold vs 2.2-fold). Overall, 3D cultures showed improved sensitivities for detecting DNA damage responses induced by the 34 compounds compared to 2D cultures.

3.8 Benchmark dose analysis of DNA damage responses in 2D and 3D HepaRG cultures

A covariate analysis was performed using PROAST. BMD_{50} values of the 15 positive DNA damage responses in 3D spheroids were divided into four groups without overlapping their 90% confidence intervals (Fig. S3A[1]). $CdCl_2$ and 4-NQO were the most potent, followed by DMNA, cisplatin, MMS, B[*a*]P, and etoposide (Tab. S1[1]). 3-MCPD and 2,4-DAT were the least potent DNA damage inducers. For 2D cultures, the 12 positive compounds were divided into three groups without overlapping their 90% confidence intervals (Fig. S3B[1]). 4-NQO, MMS, etoposide, B[*a*]P, and cisplatin were the most potent; followed by acrylamide, DMBA, ethyl acrylate, ENU, and DMNA; 3-MCPD and CPA were the least potent compounds to induce DNA strand breaks.

The exponential model was used to compare BMD values between 2D and 3D cultures (Fig. 6). For the 11 compounds that were positive in both culture models, the calculated BMD_{50} values with 90% confidence intervals overlapped for ENU, etoposide, MMS, acrylamide, B[*a*]P, and 3-MCPD in 2D and 3D cultures. The other five compounds had non-overlapping BMD_{50} values, with lower values in 3D than in 2D cultures. Specifically, the BMD_{50} values with 90% confidence intervals for 4-NQO and DMBA were next to each other, while the BMD_{50} values for cisplatin, CPA, and DMNA in 3D cultures were significantly lower than those in 2D cultures. We further compared BMD values generated from 3D HepaRG and PHH comet data of three individual donors from our previous study (donor information was presented in Tab. S2[1]) (Seo et al., 2020, 2021). Six out of the nine compounds (67%) had overlapping BMD_{50} and upper and lower confidence intervals. While the other three compounds, ENU, MMS, and DMBA, had significantly lower BMD_{50} values in PHHs than in 3D HepaRG spheroids.

4 Discussion

Growing efforts are being invested in developing new approach methodologies with the goal of reducing animal use for safety assessment of drugs and other chemicals (Parish et al., 2020). 3D spheroids have been recognized as promising *in vitro* alternative models due to their greater physiological relevance compared to 2D cultures. However, low throughput remains a concern due to technical challenges and cost. To improve the 3D assay throughput, the present study used ULA plates as a spheroid culture system and adapted the CometChip technology to 3D culture conditions for high-throughput assessment of DNA damage. It is worth noting that 384-well ULA plates provide a more cost-efficient and less time-consuming option than 96-well plates for generating large numbers of uniform spheroids reproducibly, enabling high-throughput toxicity assays. HepaRG cells were used for developing 3D cultures given that HepaRG spheroids provide a hepatocyte-like model system with physiologically relevant levels of drug metabolism, functionality, and improved sensitivity for detecting genotoxic responses compared to their 2D counterparts (Ramaiahgari et al., 2017; Mandon et al., 2019).

We first optimized the cell number and culture time of 3D spheroids by monitoring the morphology and metabolic capacity of spheroids plated at different densities (5K, 10K, and 20K cells) and cultured for up to 30 days. HepaRG spheroids retained a stable phenotype but became tighter and more compact over time (Fig. 1B). However, necrotic cores were observed in 10K and 20K spheroids at Days 10, 20, and 30 (Fig. 2A,B). The formation of a necrotic core is attributed to hypoxia due to insufficient diffusion of oxygen and nutrients in large-sized (10K and 20K) spheroids compared to small-sized (5K) spheroids (Edmondson et al., 2014). Consequently, 5K spheroids showed the highest level of albumin secretion and baseline activities for the six CYPs over a 30-day culture period, while these activities in 20K spheroids had decreased notably at Day 30 (Fig. 2D, 3A), likely due to the size- or time-dependent necrotic core formation and the loss of hepatocyte functions (Cox et al., 2020). In agreement with previous findings (Gunness et al., 2013; Leite et al., 2012; Ott et al., 2017; Ramaiahgari et al., 2017), the present study demonstrated a significantly higher liver functionality and metabolic capacity in 3D HepaRG spheroids compared to 2D cultures.

In addition to their metabolic competence, another advantage of HepaRG cells is their ability to differentiate into hepatocyte- and cholangiocyte-like cells (Le Hegarat et al., 2010). Polarized HepaRG cells in 3D spheroids form tissue-like architectures, facilitating cell-cell interactions and junctional signaling (Ramaiahgari et al., 2017). The immunofluorescent detection of CK19 (biliary epithelial cell marker) and MRP2 (canalicular marker, Fig. 2C) in 3D spheroids indicates biliary epithelial cell differentiation (Malinen et al., 2014) and the formation of bile canaliculi-like structures that are involved in the detoxification of xenobiotics (Gunness et al., 2013; Ramaiahgari et al., 2017). In addition, the expression of Ki67 demonstrates that differentiated HepaRG spheroids retain a proliferative capability, suggesting

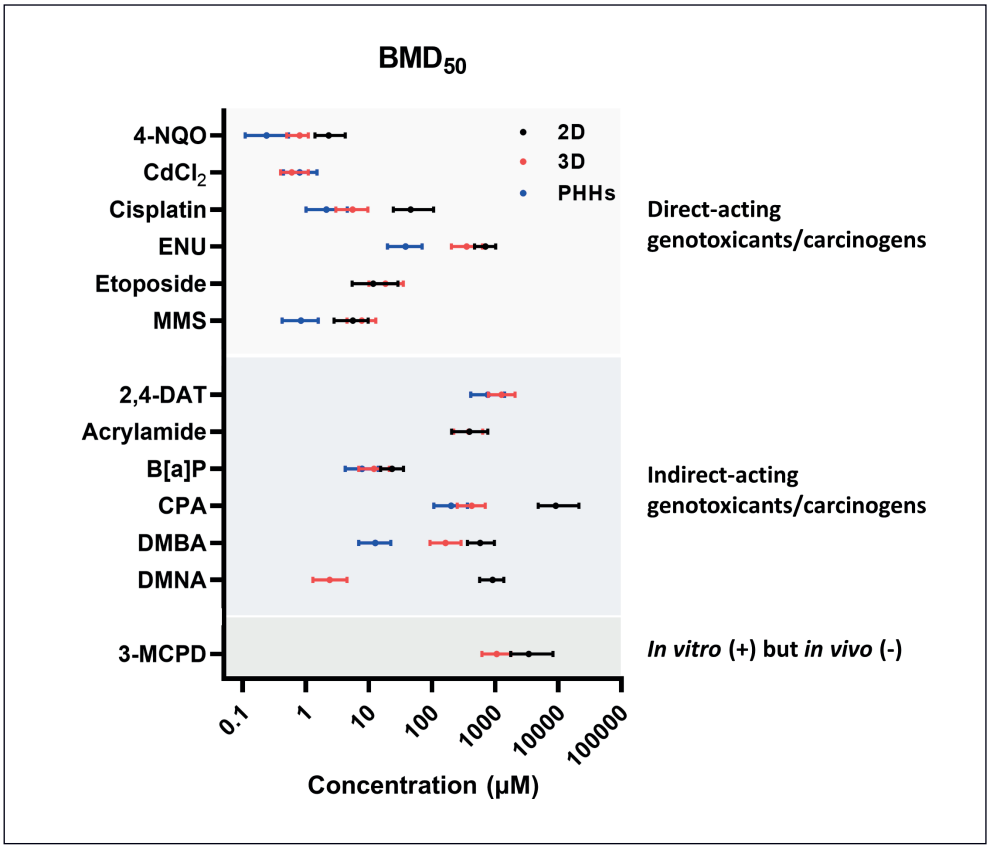

Fig. 6: Comparison of benchmark dose $(BMD)_{50}$ values with their 90% confidence intervals (BMDU and BMDL) between PHHs, 2D, and 3D HepaRG cultures
Part of the DNA damage concentration-response data in PHHs and 2D HepaRG cells was obtained from our previous studies (Seo et al. 2019, 2020). BMD_{50} values with their BMDUs and BMDLs were calculated using exponential models of PROAST. The bars represent the range between BMDUs and BMDLs and are used to differentiate between responses based on non-overlapping confidence intervals. Black, 2D HepaRG cells; Red, 3D HepaRG spheroids; Blue, PHHs. See Table 1 for abbreviations of the compounds tested.

that the spheroids may potentially be used in genotoxicity assays that require cell division, i.e., the micronucleus assay and mutation assays.

We evaluated the performance of 3D HepaRG spheroids for genotoxicity testing using two groups of compounds, i.e., 8 direct-acting and 11 indirect-acting genotoxicants/carcinogens and 15 compounds that show differing genotoxic responses *in vitro* and *in vivo* (Tab. 1). All 8 direct-acting genotoxicants/carcinogens showed similar or slight increases in cytotoxicity and DNA damage in 3D spheroids versus 2D cultures with one exception, $CdCl_2$ (Fig. 4). $CdCl_2$ was consistently negative in the 2D HepaRG comet assay (Le Hegarat et al., 2014; Seo et al., 2019), but it induced significantly increased cytotoxicity and DNA strand breaks in 3D cultures. $CdCl_2$ has been classified as a Group 1 human carcinogen by the International Agency for Research on Cancer (IARC), and several mechanisms, i.e., mainly oxidative stress and inhibition of DNA repair, are involved in its carcinogenicity (IARC, 2012; Nair et al., 2013). 3D HepaRG spheroids exhibited a similar behavior to that of PHHs in detecting the cytotoxic and genotoxic potential of $CdCl_2$ (Seo et al., 2020). CYP450 has been reported to be involved in Cd metabolism and Cd can cause increases in CYP1A1, 2B22, 7A1, and 8B1 in chicken, fish or pig (Wang et al., 2021). We speculate that increased CYP activities may contribute to the induced DNA damage in 3D spheroids.

Compared to 2D HepaRG cells, 3D spheroids showed a higher sensitivity in detecting DNA damage of the 11 indirect-acting genotoxicants/carcinogens, with three compounds (2,4-DAT, IQ, and PhIP) positive solely in 3D cultures (Fig. 4B, Tab. 2). 2,4-DAT, a hepatocarcinogenic aromatic amine, is hydroxylated by CYP1A2 and then activated via *O*-acetylation to the mutagenic metabolite 4-acetylamino-2-aminotoluene by *N*-NAT (OEHHA, 2015). CYP1A2 also is involved in the oxidation of two HAAs (IQ and PhIP), forming DNA-reactive metabolites, including *N*-hydroxy-HAAs and *N*-acetoxy-HAAs via *O*-esterification (IARC, 1993; Kirkland et al., 2016; Stampar et al., 2019). Significantly increased levels of CYP1A2 expression and activity in 3D spheroids (Fig. 3) may produce high levels of genotoxic metabolites of the three aromatic amines and subsequently induced DNA damage. In contrast, 2-AAF, another aromatic amine also hydroxylated by CYP1A2, caused slightly increased DNA damage in 3D spheroids compared to 2D cultures (1.7- vs 1.1-fold) in the present study, but this was not statistically significant (Tab. 2). However, a recent study reported a positive response of PhIP and a negative response of IQ in both 2D and 3D HepaRG cultures using the comet assay, while 2-AAF was negative in 2D but positive in 3D cultures (Mandon et al., 2019). The discrepancy between the two studies may be due to different exposure times (24 h vs 48 h) and/or weak positive responses (~10% of tail DNA) in the comet assay (Fig. 4B).

The mycotoxin AFB1 requires metabolic activation by mainly CYP3A4 and 1A2 to form a very reactive 8,9-exo-epoxide metabolite (Kirkland et al., 2016; Le Hegarat et al., 2010). Although

3D spheroids expressed significantly higher mRNA levels and activities of CYP3A4 and 1A2, AFB1 induced greater cytotoxicity but not significant DNA damage in 3D spheroids compared to 2D cultured cells. AFB1 at 2.5 and 5 µM induced statistically significant increases in % tail DNA in 2D HepaRG cells after a 3-h exposure, while extended exposures of 24-h and 52-h showed no significant increases in DNA damage (Buick et al., 2021; Le Hegarat et al., 2010). AFB1 is known to induce mainly bulky DNA damage (Weng et al., 2017), but the alkaline comet assay is not sensitive to detect potentially carcinogenic bulky adducts. A recent study reported that application of DNA synthesis inhibitors (hydroxyurea (HU) and 1-β-D-arabinofuranosyl cytosine (AraC)) significantly increased AFB1-induced DNA damage in HepaRG cells, demonstrating improved sensitivity of the CometChip assay by using HU/AraC to trap nucleotide excision repair (NER) intermediates for detecting bulky DNA adducts (Ngo et al., 2020). It requires further investigation as to whether the HU/AraC approach can be applied to other chemical classes, i.e., aromatic amines 2,4-DAT, 2-AAF, IQ, and PhIP for increasing the sensitivity of detecting bulky DNA adducts.

All five indirect-acting compounds that induced positive responses in both cultures showed similar or higher % tail DNA in 3D spheroids than in 2D HepaRG cells. Two polycyclic aromatic hydrocarbons, B[*a*]P and DMBA, are metabolically activated by CYP1A1 and 1B1 with the aid of epoxide hydrolase to form the ultimate carcinogenic metabolites, B[*a*]P-7,8-diol-9,10-epoxide and DMBA-3,4-diol-1,2-epoxide (Shimada and Fujii-Kuriyama, 2004). The two potent alkylating agents CPA and DMNA require metabolic activation by CYP2B6 and 2E1, respectively, to form highly reactive intermediate compounds that bind to the O^6-and/or N^7-position of guanine (Kirkland et al., 2016). Acrylamide is metabolized by CYP2E1 to a more DNA-reactive compound, glycidamide (Besaratinia and Pfeifer, 2007; Manjanatha et al., 2006). Increased DNA damage responses in 3D HepaRG spheroids might be explained to some extent by 2-25-fold elevated gene expression levels and/or activities of CYPs that were involved in the metabolic activation of these compounds, i.e., CYP1A1, 1B1, 2B6, and 2E1 (Fig. 3B).

We further expanded our study and tested the DNA damage potential of 15 compounds that show different genotoxic responses *in vitro* and *in vivo* and found that only one compound, 3-MCPD, was positive in both 2D and 3D cultures. 3-MCPD was mutagenic in the Ames bacterial revertant mutation assay (IARC, 2013). The compound, along with its metabolites β-chlorolactic acid and glycidol, induced DNA damage under *in vitro* conditions (Ozcagli et al., 2016). However, 3-MCPD did not increase the frequencies of MN and pig-a mutant in red blood cells as well as gpt and Spi$^-$ mutations in the kidney and testis of F344 gpt delta rats dosed with 3-MCPD 40 mg/kg bodyweight for four weeks (Onami et al., 2014). No DNA strand breaks were induced in the leukocytes, liver, kidney, testis, and bone marrow of rats dosed with 3-MCPD 60 mg/kg body weight for two days (El Ramy et al., 2007). Ethyl acrylate induced concentration-dependent increases in mutant frequency and chromosome aberrations in mouse lymphoma cells when tested without exogenous activation (Moore et al., 1988). However, it failed to induce sister chromatid exchange, DNA damage, chromosomal aberration, gpt or Spi$^-$ mutations in rodents *in vivo* (Ellis-Hutchings et al., 2018; IARC, 1999). In the present study, ethyl acrylate was more cytotoxic and increased % tail DNA in 2D cultured cells, but the increase was not significant in 3D spheroids (Fig. 5). Both 3-MCPD and ethyl acrylate induced tumors in rodents and were classified as Group 2B possible carcinogens to humans (IARC, 1999, 2013). However, ethyl acrylate is mainly metabolized by carboxylesterase-mediated hydrolysis and GSH conjugation (Ellis-Hutchings et al., 2018). Forestomach tumors observed in rodents were considered not relevant for human carcinogenicity and NTP delisted ethyl acrylate from the 9th edition of the Report on Carcinogens (Suh et al., 2018). The other eight *in vitro* (+) but *in vivo* (-) compounds were all negative in the CometChip assay conducted with 2D and 3D HepaRG models in the present study. These compounds did not induce tumors in rodents or had no *in vivo* data available (Tab. 1) (Kirkland et al., 2016). Based on these observations, we suggest that 3D HepaRG spheroids may significantly reduce the false-positive rate in current genotoxicity testing and serve as a reliable *in vitro* model in identifying compounds that indeed cause genotoxicity/carcinogenicity in humans.

Five compounds that were *in vitro* (-) but *in vivo* (+) all showed negative responses in the 3D HepaRG CometChip assay (Tab. 2, Fig. 5C). All five compounds were negative in the Ames test, but induced mutations and tumors in rodents, and 1,4-dioxane was the only compound in this group that was classified as a Group 2B possible human carcinogen by IARC (Tab. 1) (IARC, 1999). Although further investigation is required to determine whether the mutagenic and carcinogenetic effects induced by the other four compounds (dicyclanil, dimethyl terephthalate (DMTP), estragole, and leucomalachite green (LMG)) in rodents could reflect human responses, this observation demonstrates that the comet assay may not be as reliable as mutagenicity assays, i.e., pig-a assay, transgenic rodent (TGR) gene mutation assays for identifying mutagens/mutagenic carcinogens. Thus, the results provide evidence supporting that the comet assay may not be an appropriate follow-up test for *in vitro* mutagenicity assays to screen for *in vivo* mutagenicity (Robison et al., 2021).

Quantitative dose-response analysis of CometChip data using BMD modeling can promote derivation of a more precise point of departure than an LEC because the CometChip's high-throughput feature enables the generation of a large number of data points covering low concentrations (Seo et al., 2019; Wills et al., 2016). It is worth noting that two promutagens, CPA and DMNA, showed significantly lower BMD_{50} values in 3D than in 2D HepaRG cultures likely due to the increased CYP450-mediated bioactivation of the two compounds into their reactive metabolites in 3D HepaRG spheroids (Fig. 6). There was also a trend that PHHs have relatively lower or similar BMD_{50} values when compared with those generated from HepaRG comet data. In addition, we found that compared to 2D cultured cells, 3D spheroids had BMD_{50} values that were much closer to those of PHHs for almost all the compounds tested. These results suggest that 3D HepaRG spheroids more closely resemble PHHs than 2D HepaRG cells for generating DNA

damage dose-response data. Therefore, for quantitative purposes, 3D HepaRG models might be preferred over 2D cultures to generate data for estimating health-based guidance values using quantitative *in vitro* to *in vivo* extrapolation approaches for human health risk assessment.

In conclusion, 3D HepaRG spheroids provide a useful hepatocyte-like *in vitro* model system with increased metabolic capacity and functionality compared to 2D HepaRG cells. The CometChip technology facilitates a high-throughput application of 3D HepaRG models. The improved sensitivity for detecting DNA damage responses of known genotoxicants/carcinogens in 3D spheroids suggests that 3D HepaRG spheroids predict *in vivo* genotoxicity responses better. Quantitative analysis using high-throughput dose-response data from 3D HepaRG spheroids generated BMD values close to those in PHHs. Overall, the developed *in vitro* system using metabolically competent 3D HepaRG spheroids can enhance the performance of *in vitro* genotoxicity testing by generating data that are more relevant to the human metabolic condition. Since chemicals may cause genotoxicity via various mechanisms (i.e., DNA damage, chromosomal aberration, and mutation), and the comet assay detects only DNA strand breaks, an integrated test battery that measures different genotoxicity endpoints using metabolically competent human hepatocyte spheroids is warranted for providing information for appropriate follow-up *in vivo* testing, thus reducing unnecessary animal studies.

References

Baharvand, H., Hashemi, S. M., Kazemi Ashtiani, S. et al. (2006). Differentiation of human embryonic stem cells into hepatocytes in 2D and 3D culture systems in vitro. *Int J Dev Biol 50*, 645-652. doi:10.1387/ijdb.052072hb

Bemis, J. C., Avlasevich, S. L., Labash, C. et al. (2018). Glycosylphosphatidylinositol (GPI) anchored protein deficiency serves as a reliable reporter of Pig-a gene mutation: Support from an in vitro assay based on L5178Y/Tk$^{+/-}$ cells and the CD90.2 antigen. *Environ Mol Mutagen 59*, 18-29. doi:10.1002/em.22154

Besaratinia, A. and Pfeifer, G. P. (2007). A review of mechanisms of acrylamide carcinogenicity. *Carcinogenesis 28*, 519-528. doi:10.1093/carcin/bgm006

Bhalli, J. A., Shaddock, J. G., Pearce, M. G. et al. (2013). Sensitivity of the Pig-a assay for detecting gene mutation in rats exposed acutely to strong clastogens. *Mutagenesis 28*, 447-455. doi:10.1093/mutage/get022

Breslin, S. and O'Driscoll, L. (2013). Three-dimensional cell culture: The missing link in drug discovery. *Drug Discov Today 18*, 240-249. doi:10.1016/j.drudis.2012.10.003

Buick, J. K., Williams, A., Meier, M. J. et al. (2021). A modern genotoxicity testing paradigm: Integration of the high-throughput cometchip® and the TGx-DDI transcriptomic biomarker in human HhepaRG™ cell cultures. *Front Public Health 9*, 694834. doi:10.3389/fpubh.2021.694834

Chao, C. and Engelward, B. P. (2020). Applications of cometchip for environmental health studies. *Chem Res Toxicol 33*, 1528-1538. doi:10.1021/acs.chemrestox.9b00393

Conway, G. E., Shah, U. K., Llewellyn, S. et al. (2020). Adaptation of the in vitro micronucleus assay for genotoxicity testing using 3D liver models supporting longer-term exposure durations. *Mutagenesis 35*, 319-330. doi:10.1093/mutage/geaa018

Cox, C. R., Lynch, S., Goldring, C. et al. (2020). Current perspective: 3D spheroid models utilizing human-based cells for investigating metabolism-dependent drug-induced liver injury. *Front Med Technol 2*, 611913. doi:10.3389/fmedt.2020.611913

Culp, S. J. (2004). NTP technical report on the toxicity studies of malachite green chloride and leucomalachite green (CAS Nos. 569-64-2 and 129-73-7) administered in feed to F344/N rats and B6C3F1 mice. *Toxic Rep Ser*, 1-F10.

Custer, L., Roberts, D., and Nicotra, S. (2015). In vivo follow-up testing for in vitro mutagenic and clastogenic reagents EDAC and HOPO. *Abstracts from the Environmental Mutagenesis and Genomics Society, 46th Annual Meeting*. *Environ Mol Mutagen 56*, S44. doi:10.1002/em.21969

David, R., Talbot, E., Allen, B. et al. (2018). The development of an in vitro Pig-a assay in L5178Y cells. *Arch Toxicol 92*, 1609-1623. doi:10.1007/s00204-018-2157-4

Dertinger, S. D., Phonethepswath, S., Avlasevich, S. L. et al. (2012). Efficient monitoring of in vivo Pig-a gene mutation and chromosomal damage: Summary of 7 published studies and results from 11 new reference compounds. *Toxicol Sci 130*, 328-348. doi:10.1093/toxsci/kfs258

Dertinger, S. D., Avlasevich, S. L., Torous, D. K. et al. (2019). 3Rs friendly study designs facilitate rat liver and blood micronucleus assays and Pig-a gene mutation assessments: Proof-of-concept with 13 reference chemicals. *Environ Mol Mutagen 60*, 704-739. doi:10.1002/em.22312

Ding, W., Levy, D. D., Bishop, M. E. et al. (2015). In vivo genotoxicity of estragole in male F344 rats. *Environ Mol Mutagen 56*, 356-365. doi:10.1002/em.21918

Dobo, K. L., Cheung, J. R., Gunther, W. C. et al. (2018). 2-hydroxypyridine-N-oxide (HOPO): Equivocal in the ames assay. *Environ Mol Mutagen 59*, 312-321. doi:10.1002/em.22179

Dobo, K. L., Coffing, S., Gunther, W. C. et al. (2019). 2-hydroxypyridine n-oxide is not genotoxic in vivo. *Environ Mol Mutagen 60*, 588-593. doi:10.1002/em.22294

ECHA, T. E. C. A. (2021). N'-(ethylcarbonimidoyl)-N, N-dimethylpropane-1,3-diamine monohydrochloride. https://echa.europa.eu/registration-dossier/-/registered-dossier/23229/23227/23227/23221

Edmondson, R., Broglie, J. J., Adcock, A. F. et al. (2014). Three-dimensional cell culture systems and their applications in drug discovery and cell-based biosensors. *Assay Drug Dev Technol 12*, 207-218. doi:10.1089/adt.2014.573

EFSA, S. C., Hardy, A., Benford, D. et al. (2017). Update: Use of the benchmark dose approach in risk assessment. *EFSA J 15*, e04658. doi:10.2903/j.efsa.2017.4658

Eichenbaum, G., Johnson, M., Kirkland, D. et al. (2009). Assessment of the genotoxic and carcinogenic risks of p-nitrophenol when it is present as an impurity in a drug product. *Regul Toxicol Pharmacol 55*, 33-42. doi:10.1016/j.yrtph.2009.05.018

El Ramy, R., Ould Elhkim, M., Lezmi, S. et al. (2007). Evaluation of the genotoxic potential of 3-monochloropropane-1,2-diol (3-MCPD) and its metabolites, glycidol and beta-chlorolactic acid, using the single cell gel/comet assay. *Food Chem Toxicol 45*, 41-48. doi:10.1016/j.fct.2006.07.014

Elia, M. C., Storer, R. D., McKelvey, T. W. et al. (1994). Rapid DNA degradation in primary rat hepatocytes treated with diverse cytotoxic chemicals: Analysis by pulsed field gel electrophoresis and implications for alkaline elution assays. *Environ Mol Mutagen 24*, 181-191. doi:10.1002/em.2850240307

Elje, E., Hesler, M., Runden-Pran, E. et al. (2019). The comet assay applied to HepG2 liver spheroids. *Mutat Res Genet Toxicol Environ Mutagen 845*, 403033. doi:10.1016/j.mrgentox.2019.03.006

Ellis-Hutchings, R., Giuliani, J., Hayashi, M. et al. (2018). The role of ethyl acrylate induced GSH depletion in the rodent forestomach and its impact on MTD and in vivo genotoxicity in developing an adverse outcome pathway (AOP). *Regul Toxicol Pharmacol 92*, 173-181. doi:10.1016/j.yrtph.2017.11.012

FDA/CDER (2013). Pharmacology Review(s): Secondary pharmacology and toxicology review for NDA 204-820. https://www.accessdata.fda.gov/drugsatfda_docs/nda/2014/204820Orig1s000PharmR.pdf

Fowler, P., Smith, K., Young, J. et al. (2012). Reduction of misleading ("false") positive results in mammalian cell genotoxicity assays. I. Choice of cell type. *Mutat Res 742*, 11-25. doi:10.1016/j.mrgentox.2011.10.014

Gi, M., Fujioka, M., Kakehashi, A. et al. (2018). In vivo positive mutagenicity of 1,4-dioxane and quantitative analysis of its mutagenicity and carcinogenicity in rats. *Arch Toxicol 92*, 3207-3221. doi:10.1007/s00204-018-2282-0

Goncharova, R. I., Zabrejko, S., Kozachenko, V. I. et al. (1988). Mutagenic effects of dimethyl terephthalate on mouse somatic cells in vivo. *Mutat Res 204*, 703-709. doi:10.1016/0165-1218(88)90076-6

Graupner, A., Instanes, C., Dertinger, S. D. et al. (2014). Single cell gel electrophoresis (SCGE) and Pig-a mutation assay in vivo-tools for genotoxicity testing from a regulatory perspective: A study of benzo[a]pyrene in Ogg1(-/-) mice. *Mutat Res Genet Toxicol Environ Mutagen 772*, 34-41. doi:10.1016/j.mrgentox.2014.07.010

Guillouzo, A., Corlu, A., Aninat, C. et al. (2007). The human hepatoma heparg cells: A highly differentiated model for studies of liver metabolism and toxicity of xenobiotics. *Chem Biol Interact 168*, 66-73. doi:10.1016/j.cbi.2006.12.003

Gunness, P., Mueller, D., Shevchenko, V. et al. (2013). 3D organotypic cultures of human heparg cells: A tool for in vitro toxicity studies. *Toxicol Sci 133*, 67-78. doi:10.1093/toxsci/kft021

Guo, X., Heflich, R. H., Dial, S. L. et al. (2016). Quantitative analysis of the relative mutagenicity of five chemical constituents of tobacco smoke in the mouse lymphoma assay. *Mutagenesis 31*, 287-296. doi:10.1093/mutage/gev039

Guo, X., Seo, J. E., Petibone, D. et al. (2020). Performance of HepaRG and HepG2 cells in the high-throughput micronucleus assay for in vitro genotoxicity assessment. *J Toxicol Environ Health A 83*, 702-717. doi:10.1080/15287394.2020.1822972

Habas, K., Brinkworth, M. H. and Anderson, D. (2017). In vitro responses to known in vivo genotoxic agents in mouse germ cells. *Environ Mol Mutagen 58*, 99-107. doi:10.1002/em.22075

Hartmann, A. and Speit, G. (1997). The contribution of cytotoxicity to DNA-effects in the single cell gel test (comet assay). *Toxicol Lett 90*, 183-188. doi:10.1016/s0378-4274(96)03847-7

Hu, T., Kaluzhny, Y., Mun, G. C. et al. (2009). Intralaboratory and interlaboratory evaluation of the EpiDerm 3D human reconstructed skin micronucleus (RSMN) assay. *Mutat Res 673*, 100-108. doi:10.1016/j.mrgentox.2008.12.003

IARC (1993). Some naturally occurring substances: Food items and constituents, heterocyclic aromatic amines and mycotoxins. *IARC Monogr Eval Carcinog Risks Hum 56*, 165-242.

IARC (1994). Some industrial chemicals. *IARC Monogr Eval Carcinog Risks Hum 60*, 389-433.

IARC (1999). Re-evaluation of some organic chemicals, hydrazine and hydrogen peroxide. *IARC Monogr Eval Carcinog Risks Hum 71*.

IARC (2000). Some antiviral and antineoplastic drugs, and other pharmaceutical agents. *IARC Monogr Eval Carcinog Risks Hum 76*.

IARC (2012). Arsenic, metals, fibres, and dusts. *IARC Monogr Eval Carcinog Risks Hum 100C*, 121-145.

IARC (2013). Some chemicals present in industrial and consumer products, food and drinking-water. *IARC Monogr Eval Carcinog Risks Hum 101*, 9-549.

IARC (2019a). Isobutyl nitrite, beta-picoline, and some acrylates. *IARC Monogr Eval Carcinog Risks Hum 122*, 97-135.

IARC (2019b). Styrene, styrene-7,8-oxide, and quinoline. *IARC Monogr Eval Carcinog Risks Hum 121*, 37-295.

Itoh, S. and Hattori, C. (2019). In vivo genotoxicity of 1,4-dioxane evaluated by liver and bone marrow micronucleus tests and Pig-a assay in rats. *Mutat Res Genet Toxicol Environ Mutagen 837*, 8-14. doi:10.1016/j.mrgentox.2018.09.004

Ivanov, D. P., Parker, T. L., Walker, D. A. et al. (2014). Multiplexing spheroid volume, resazurin and acid phosphatase viability assays for high-throughput screening of tumour spheroids and stem cell neurospheres. *PLoS One 9*, e103817. doi:10.1371/journal.pone.0103817

Kanojia, D. and Vaidya, M. M. (2006). 4-nitroquinoline-1-oxide induced experimental oral carcinogenesis. *Oral Oncol 42*, 655-667. doi:10.1016/j.oraloncology.2005.10.013

Kirkland, D., Pfuhler, S., Tweats, D. et al. (2007). How to reduce false positive results when undertaking in vitro genotoxicity testing and thus avoid unnecessary follow-up animal tests: Report of an ECVAM workshop. *Mutat Res 628*, 31-55. doi:10.1016/j.mrgentox.2006.11.008

Kirkland, D. (2011). Improvements in the reliability of in vitro genotoxicity testing. *Expert Opin Drug Metab Toxicol 7*, 1513-1520. doi:10.1517/17425255.2011.627855

Kirkland, D., Kasper, P., Martus, H. J. et al. (2016). Updated re-

commended lists of genotoxic and non-genotoxic chemicals for assessment of the performance of new or improved genotoxicity tests. *Mutat Res Genet Toxicol Environ Mutagen 795*, 7-30. doi:10.1016/j.mrgentox.2015.10.006

Kirkland, D., Uno, Y., Luijten, M. et al. (2019). In vivo genotoxicity testing strategies: Report from the 7th international workshop on genotoxicity testing (IWGT). *Mutat Res Genet Toxicol Environ Mutagen 847*, 403035. doi:10.1016/j.mrgentox.2019.03.008

Koppen, G., Azqueta, A., Pourrut, B. et al. (2017). The next three decades of the comet assay: A report of the 11th international comet assay workshop. *Mutagenesis 32*, 397-408. doi:10.1093/mutage/gex002

Lauschke, V. M., Hendriks, D. F., Bell, C. C. et al. (2016). Novel 3D culture systems for studies of human liver function and assessments of the hepatotoxicity of drugs and drug candidates. *Chem Res Toxicol 29*, 1936-1955. doi:10.1021/acs.chemrestox.6b00150

Le Hegarat, L., Dumont, J., Josse, R. et al. (2010). Assessment of the genotoxic potential of indirect chemical mutagens in HepaRG cells by the comet and the cytokinesis-block micronucleus assays. *Mutagenesis 25*, 555-560. doi:10.1093/mutage/geq039

Le Hegarat, L., Mourot, A., Huet, S. et al. (2014). Performance of comet and micronucleus assays in metabolic competent HepaRG cells to predict in vivo genotoxicity. *Toxicol Sci 138*, 300-309. doi:10.1093/toxsci/kfu004

Leite, S. B., Wilk-Zasadna, I., Zaldivar, J. M. et al. (2012). Three-dimensional HepaRG model as an attractive tool for toxicity testing. *Toxicol Sci 130*, 106-116. doi:10.1093/toxsci/kfs232

Liu, W., Xi, J., Cao, Y. et al. (2019). An adaption of human-induced hepatocytes to in vitro genetic toxicity tests. *Mutagenesis 34*, 165-171. doi:10.1093/mutage/gey041

Malinen, M. M., Kanninen, L. K., Corlu, A. et al. (2014). Differentiation of liver progenitor cell line to functional organotypic cultures in 3D nanofibrillar cellulose and hyaluronan-gelatin hydrogels. *Biomaterials 35*, 5110-5121. doi:10.1016/j.biomaterials.2014.03.020

Mandon, M., Huet, S., Dubreil, E. et al. (2019). Three-dimensional HepaRG spheroids as a liver model to study human genotoxicity in vitro with the single cell gel electrophoresis assay. *Sci Rep 9*, 10548. doi:10.1038/s41598-019-47114-7

Manjanatha, M. G., Aidoo, A., Shelton, S. D. et al. (2006). Genotoxicity of acrylamide and its metabolite glycidamide administered in drinking water to male and female big blue mice. *Environ Mol Mutagen 47*, 6-17. doi:10.1002/em.20157

Martins, C., Cacao, R., Cole, K. J. et al. (2012). Estragole: A weak direct-acting food-borne genotoxin and potential carcinogen. *Mutat Res 747*, 86-92. doi:10.1016/j.mrgentox.2012.04.009

Masuda-Herrera, M. J., Dobo, K. L., Kenyon, M. O. et al. (2019). In vivo mutagenicity testing of arylboronic acids and esters. *Environ Mol Mutagen 60*, 766-777. doi:10.1002/em.22320

Mittelstaedt, R. A., Mei, N., Webb, P. J. et al. (2004). Genotoxicity of malachite green and leucomalachite green in female Big Blue B6C3F1 mice. *Mutat Res 561*, 127-138. doi:10.1016/j.mrgentox.2004.04.003

Monarca, S., Pool-Zobel, B. L., Rizzi, R. et al. (1991). In vitro genotoxicity of dimethyl terephthalate. *Mutat Res 262*, 85-92. doi:10.1016/0165-7992(91)90112-h

Moore, M. M., Amtower, A., Doerr, C. L. et al. (1988). Genotoxicity of acrylic acid, methyl acrylate, ethyl acrylate, methyl methacrylate, and ethyl methacrylate in L5178Y mouse lymphoma cells. *Environ Mol Mutagen 11*, 49-63. doi:10.1002/em.2850110107

Moore, M. M., Pottenger, L. H. and House-Knight, T. (2019). Critical review of styrene genotoxicity focused on the mutagenicity/clastogenicity literature and using current organization of economic cooperation and development guidance. *Environ Mol Mutagen 60*, 624-663. doi:10.1002/em.22278

Morita, T. and Hayashi, M. (1998). 1,4-dioxane is not mutagenic in five in vitro assays and mouse peripheral blood micronucleus assay, but is in mouse liver micronucleus assay. *Environ Mol Mutagen 32*, 269-280. doi:10.1002/(sici)1098-2280(1998)32:3<269::aid-em10>3.0.co;2-8

Morita, T., Hamada, S., Masumura, K. et al. (2016). Evaluation of the sensitivity and specificity of in vivo erythrocyte micronucleus and transgenic rodent gene mutation tests to detect rodent carcinogens. *Mutat Res Genet Toxicol Environ Mutagen 802*, 1-29. doi:10.1016/j.mrgentox.2016.03.008

Muller, L., Kasper, P., Muller-Tegethoff, K. et al. (1994). The genotoxic potential in vitro and in vivo of the allyl benzene etheric oils estragole, basil oil and trans-anethole. *Mutat Res 325*, 129-136. doi:10.1016/0165-7992(94)90075-2

Nair, A. R., Degheselle, O., Smeets, K. et al. (2013). Cadmium-induced pathologies: Where is the oxidative balance lost (or not)? *Int J Mol Sci 14*, 6116-6143. doi:10.3390/ijms14036116

Ngo, L. P., Owiti, N. A., Swartz, C. et al. (2020). Sensitive cometchip assay for screening potentially carcinogenic DNA adducts by trapping DNA repair intermediates. *Nucleic Acids Res 48*, e13. doi:10.1093/nar/gkz1077

Nohmi, T. (2018). Thresholds of genotoxic and non-genotoxic carcinogens. *Toxicol Res 34*, 281-290. doi:10.5487/TR.2018.34.4.281

NTP (1993). Toxicology and carcinogenesis studies of *p*-nitrophenol (cas no. 100-02-7) in swiss-webster mice (dermal studies). *Natl Toxicol Program Tech Rep Ser 417*, 1-161. https://ntp.niehs.nih.gov/ntp/htdocs/lt_rpts/tr417.pdf

NTP (1998). NTP toxicology and carcinogenesis studies of technical grade sodium xylenesulfonate (cas no. 1300-72-7) in F344/N rats and B6C3F1 mice (dermal studies). *Natl Toxicol Program Tech Rep Ser 464*, 1-272. https://www.ncbi.nlm.nih.gov/pubmed/12579200

NTP (2022a). Testing Status of Dimethyl terephthalate 10553-L. https://ntp.niehs.nih.gov/go/ts-10553-l

NTP (2022b). Testing Status of 1,4-Dioxane 10568-P *(TR-080)*. https://ntp.niehs.nih.gov/go/ts-10568-p

NTP (2022c). Testing Status of Phthalic anhydride 10421-A. https://ntp.niehs.nih.gov/go/ts-10421-a

OECD (2017). Overview on genetic toxicology TGs. *OECD Series on Testing and Assessment, No. 238*. OECD Publishing, Paris. doi:10.1787/9789264274761-en

OECD (2020). The in vivo erythrocyte Pig-a gene mutation assay – Part 1 – Detailed Review Paper and Retrospective Performance Assessment. *Series on Testing and Assessment, No. 315*. https://www.oecd.org/officialdocuments/publicdisplaydocumentpdf/?cote=env/jm/mono(2020)6&doclanguage=en

OEHHA (2015). Diaminotoluenes (DATs). The Office of Environmental Health Hazard Assessment (OEHHA). https://oehha.ca.gov/media/downloads/proposition-65/chemicals/082815diaminotolueneshid.pdf

Onami, S., Cho, Y. M., Toyoda, T. et al. (2014). Absence of in vivo genotoxicity of 3-monochloropropane-1,2-diol and associated fatty acid esters in a 4-week comprehensive toxicity study using F344 gpt delta rats. *Mutagenesis 29*, 295-302. doi:10.1093/mutage/geu018

Ott, L. M., Ramachandran, K. and Stehno-Bittel, L. (2017). An automated multiplexed hepatotoxicity and CYP induction assay using heparg cells in 2D and 3D. *SLAS Discov 22*, 614-625. doi:10.1177/2472555217701058

Ozcagli, E., Alpertunga, B., Fenga, C. et al. (2016). Effects of 3-monochloropropane-1,2-diol (3-MCPD) and its metabolites on DNA damage and repair under in vitro conditions. *Food Chem Toxicol 89*, 1-7. doi:10.1016/j.fct.2015.12.027

Parish, S. T., Aschner, M., Casey, W. et al. (2020). An evaluation framework for new approach methodologies (NAMs) for human health safety assessment. *Regul Toxicol Pharmacol 112*, 104592. doi:10.1016/j.yrtph.2020.104592

Peng, C., Arthur, D., Liu, F. et al. (2013). Genotoxicity of hydroquinone in A549 cells. *Cell Biol Toxicol 29*, 213-227. doi:10.1007/s10565-013-9247-0

Pfuhler, S., Fellows, M., van Benthem, J. et al. (2011). In vitro genotoxicity test approaches with better predictivity: Summary of an IWGT workshop. *Mutat Res 723*, 101-107. doi:10.1016/j.mrgentox.2011.03.013

Pfuhler, S., van Benthem, J., Curren, R. et al. (2020). Use of in vitro 3D tissue models in genotoxicity testing: Strategic fit, validation status and way forward. Report of the working group from the 7th international workshop on genotoxicity testing (IWGT). *Mutat Res Genet Toxicol Environ Mutagen 850-851*, 503135. doi:10.1016/j.mrgentox.2020.503135

Przybojewska, B., Dziubaltowska, E. and Kowalski, Z. (1984). Genotoxic effects of ethyl acrylate and methyl acrylate in the mouse evaluated by the micronucleus test. *Mutat Res 135*, 189-191. doi:10.1016/0165-1218(84)90120-4

Ramaiahgari, S. C., Waidyanatha, S., Dixon, D. et al. (2017). From the cover: Three-dimensional (3D) HepaRG spheroid model with physiologically relevant xenobiotic metabolism competence and hepatocyte functionality for liver toxicity screening. *Toxicol Sci 159*, 124-136. doi:10.1093/toxsci/kfx122

Robison, T. W., Heflich, R. H., Manjanatha, M. G. et al. (2021). Appropriate in vivo follow-up assays to an in vitro bacterial reverse mutation (ames) test positive investigational drug candidate (active pharmaceutical ingredient), drug-related metabolite, or drug-related impurity. *Mutat Res Genet Toxicol Environ Mutagen 868-869*, 503386. doi:10.1016/j.mrgentox.2021.503386

Schulte-Hubbert, R., Kupper, J. H., Thomas, A. D. et al. (2020). Estragole: DNA adduct formation in primary rat hepatocytes and genotoxic potential in HepG2-CYP1A2 cells. *Toxicology 444*, 152566. doi:10.1016/j.tox.2020.152566

Seo, J. E., Tryndyak, V., Wu, Q. et al. (2019). Quantitative comparison of in vitro genotoxicity between metabolically competent heparg cells and HepG2 cells using the high-throughput high-content cometchip assay. *Arch Toxicol 93*, 1433-1448. doi:10.1007/s00204-019-02406-9

Seo, J. E., Wu, Q., Bryant, M. et al. (2020). Performance of high-throughput cometchip assay using primary human hepatocytes: A comparison of DNA damage responses with in vitro human hepatoma cell lines. *Arch Toxicol 94*, 2207-2224. doi:10.1007/s00204-020-02736-z

Seo, J. E., Davis, K., Malhi, P. et al. (2021). Genotoxicity evaluation using primary hepatocytes isolated from rhesus macaque (Macaca mulatta). *Toxicology 462*, 152936. doi:10.1016/j.tox.2021.152936

Severin, I., Jondeau, A., Dahbi, L. et al. (2005). 2,4-diaminotoluene (2,4-dat)-induced DNA damage, DNA repair and micronucleus formation in the human hepatoma cell line HepG2. *Toxicology 213*, 138-146. doi:10.1016/j.tox.2005.05.021

Shah, U. K., Seager, A. L., Fowler, P. et al. (2016). A comparison of the genotoxicity of benzo[a]pyrene in four cell lines with differing metabolic capacity. *Mutat Res Genet Toxicol Environ Mutagen 808*, 8-19. doi:10.1016/j.mrgentox.2016.06.009

Shah, U. K., Mallia, J. O., Singh, N. et al. (2018). A three-dimensional in vitro HepG2 cells liver spheroid model for genotoxicity studies. *Mutat Res Genet Toxicol Environ Mutagen 825*, 51-58. doi:10.1016/j.mrgentox.2017.12.005

Shelby, M. D., Erexson, G. L., Hook, G. J. et al. (1993). Evaluation of a three-exposure mouse bone marrow micronucleus protocol: Results with 49 chemicals. *Environ Mol Mutagen 21*, 160-179. doi:10.1002/em.2850210210

Shi, J., Krsmanovic, L., Bruce, S. et al. (2011). Assessment of genotoxicity induced by 7,12-dimethylbenz(a)anthracene or diethylnitrosamine in the Pig-a, micronucleus and comet assays integrated into 28-day repeat dose studies. *Environ Mol Mutagen 52*, 711-720. doi:10.1002/em.20678

Shigano, M., Ishii, N., Takashima, R. et al. (2016). Results of rat Pig-a/PIGRET assay with a single dose regimen of 1,3-propane sultone and 2-acetyl aminofluorene. *Mutat Res Genet Toxicol Environ Mutagen 811*, 75-79. doi:10.1016/j.mrgentox.2016.04.001

Shimada, T. and Fujii-Kuriyama, Y. (2004). Metabolic activation of polycyclic aromatic hydrocarbons to carcinogens by cytochromes P450 1A1 and 1B1. *Cancer Sci 95*, 1-6. doi:10.1111/j.1349-7006.2004.tb03162.x

Slob, W. (2017). A general theory of effect size, and its consequences for defining the benchmark response (BMR) for continuous endpoints. *Crit Rev Toxicol 47*, 342-351. doi:10.1080/10408444.2016.1241756

Smart, D. J., Ahmedi, K. P., Harvey, J. S. et al. (2011). Genotoxicity screening via the γH2AX by flow assay. *Mutat Res 715*, 25-31. doi:10.1016/j.mrfmmm.2011.07.001

Stampar, M., Tomc, J., Filipic, M. et al. (2019). Development of in vitro 3D cell model from hepatocellular carcinoma (HepG2) cell line and its application for genotoxicity testing. *Arch Toxicol 93*, 3321-3333. doi:10.1007/s00204-019-02576-6

Suh, M., Proctor, D., Chappell, G. et al. (2018). A review of the genotoxic, mutagenic, and carcinogenic potentials of several lower acrylates. *Toxicology 402-403*, 50-67. doi:10.1016/j.tox.2018.04.006

Umemura, T., Kuroiwa, Y., Tasaki, M. et al. (2007). Detection of oxidative DNA damage, cell proliferation and in vivo mutagenicity induced by dicyclanil, a non-genotoxic carcinogen, using gpt delta mice. *Mutat Res 633*, 46-54. doi:10.1016/j.mrgentox.2007.05.007

Villarini, M., Pagiotti, R., Dominici, L. et al. (2014). Investigation of the cytotoxic, genotoxic, and apoptosis-inducing effects of estragole isolated from fennel (Foeniculum vulgare). *J Nat Prod 77*, 773-778. doi:10.1021/np400653p

Wang, H., Han, Q., Chen, Y. et al. (2021). Novel insights into cytochrome P450 enzyme and solute carrier families in cadmium-induced liver injury of pigs. *Ecotoxicol Environ Saf 211*, 111910. doi:10.1016/j.ecoenv.2021.111910

Wang, Y., Revollo, J., McKinzie, P. et al. (2018). Establishing a novel Pig-a gene mutation assay in L5178YTk$^{+/-}$ mouse lymphoma cells. *Environ Mol Mutagen 59*, 4-17. doi:10.1002/em.22152

Weng, M. W., Lee, H. W., Choi, B. et al. (2017). AFB1 hepatocarcinogenesis is via lipid peroxidation that inhibits DNA repair, sensitizes mutation susceptibility and induces aldehyde-DNA adducts at p53 mutational hotspot codon 249. *Oncotarget 8*, 18213-18226. doi:10.18632/oncotarget.15313

WHO (2021). Toxicological evaluation of certain veterinary drug residues in food. *WHO Food Additives Series 45*. http://www.inchem.org/documents/jecfa/jecmono/v45je04.htm

Wills, J. W., Long, A. S., Johnson, G. E. et al. (2016). Empirical analysis of BMD metrics in genetic toxicology part II: In vivo potency comparisons to promote reductions in the use of experimental animals for genetic toxicity assessment. *Mutagenesis 31*, 265-275. doi:10.1093/mutage/gew009

Yamamoto, M. and Wakata, A. (2016). Evaluation of in vivo gene mutation with etoposide using Pig-a and PIGRET assays. *Mutat Res Genet Toxicol Environ Mutagen 811*, 29-34. doi:10.1016/j.mrgentox.2016.06.006

Yusuf, A. T., Vian, L., Sabatier, R. et al. (2000). In vitro detection of indirect-acting genotoxins in the comet assay using Hep G2 cells. *Mutat Res 468*, 227-234. doi:10.1016/s1383-5718(00)00052-8

Conflict of interest

The authors declare that they have no conflict of interest.

Data availability

Supplementary materials are available upon request from the corresponding author.

Acknowledgements

This study was supported by the U.S. Food and Drug Administration (FDA), National Center for Toxicological Research (NCTR, project number E0773701). J.E.S. was supported by appointments to the Postgraduate Research Program at the National Center for Toxicological Research (NCTR) administered by the Oak Ridge Institute for Science Education through an interagency agreement between the U.S. Department of Energy and the U.S. Food and Drug Administration (FDA). We greatly appreciate Drs Javier Revollo and Qiangen Wu for their critical review of this article.